Micromechanics modeling of the uniaxial strain-sensing property of carbon nanotube cement-matrix composites for SHM applications

Enrique García-Macías[a,*], Antonella D'Alessandro[b], Rafael Castro-Triguero[c], Domingo Pérez-Mira[d], Filippo Ubertini[b]

[a]*Department of Continuum Mechanics and Structural Analysis, School of Engineering, University of Seville , Camino de los Descubrimientos s/n, E-41092-Seville, Spain*
[b]*Department of Civil and Environmental Engineering, University of Perugia, Via G Duranti 93, Perugia 06125, Italy*
[c]*Department of Mechanics, University of Cordoba, Campus de Rabanales, Cordoba, CP 14071, Spain*
[d]*Department of R&D, Construcciones AZVI, Seville, Spain.*

Abstract

Recent advances in the field of Nanotechnology have made possible the development of new smart materials, among which Carbon NanoTube (CNT) cement-based composites are attracting an increasing attention. These composites exhibit strain-sensing capabilities providing measurable variations of their electrical properties under applied mechanical deformations. This unique property, together with the similarity between these composites and structural concrete, suggests the possibility of developing distributed strain-sensing systems with substantial improvements in the cost-effectiveness of large-scale concrete structures. In order to design and optimize self-sensing CNT-based composites, it is therefore essential to develop theoretical models capable of simulating the relationship between external mechanical strains and the effective electrical conductivity. This paper presents a micromechanics model to predict the piezoresistive properties of CNT cement-based nanocomposites, with the consideration of waviness and non-uniform distributions of nanoinclusions. The origin of the piezoresistive response is attributed to (i) strain-induced changes in the volume fraction, (ii) filler reorientation and, (iii) changes in the tunneling resistance. In order to count on an experimental basis to use as benchmark for validation, several nanocomposite cement-based specimens are manufactured and tested under uniaxial compression.

Keywords:
Carbon nanotube, Cement-matrix composites, Piezoresistive modeling, Percolation, Smart concrete, Structural Health Monitoring

1. Introduction

The great economic, social and environmental impacts of civil infrastructures make preventive maintenance vital for structural engineering. The field of SHM encompasses a wide range of techniques which enable timely inspection and maintenance, resulting in enhanced serviceability and longer life-cycle of structures [1, 2]. Nonetheless, the inherent size of civil structures makes existing monitoring systems hardly applicable to the large scale, which is often termed the "scalability issue" of SHM. Recent advances in the field of Nanotechnology have led to the development of new multifunctional and smart materials. In particular, electrically conductive Carbon NanoTube (CNT) cement-based composites open a vast field of applications in SHM [3–5]. These composites exhibit strain-sensing capabilities by means of measurable variations of their electrical properties under applied mechanical deformations [6–8]. This unique property, coupled with the similarity between these composites and structural concrete, suggests the possibility of developing distributed strain-sensing systems that would entail substantial improvements in the cost-effectiveness of large-scale concrete structures [9–15]. Moreover, cementitious materials also have the same durability as the monitored structure, which allows long-term applications. Many researchers have reported the exceptional mechanical enhancements of CNTs used as fillers in nanocomposites [16–20]. However, work reporting about the development of theoretical models capable of simulating the relationship between external mechanical strains and the effective electrical conductivity is still scant.

Over the last decade, many experimental results have put in evidence the percolation-like nature of the electrical conductivity of cement-based composites [21–23]. The reason of this behavior has been attributed to two

*Corresponding author.
Email address: egarcia28@us.es (Enrique García-Macías)

different conductive mechanisms: electron hopping (or quantum tunneling) and conductive networking [21, 24–26]. Below percolation, only the transfer of electrons intra-tube or tube-tube is possible due to the great distances among CNTs. However, the higher is the concentration of CNTs, the closer nanotubes may be found until adjacent fibers touch one another resulting in a continuous electrically microscale conductive path. Despite acting simultaneously, the conductivity of composites with CNT concentrations above the percolation threshold is believed to be dominated by conductive networks. Hence, the origin of the self-sensing property is due to the tampering of these mechanisms induced by external mechanical strains. In particular, three major expected changes during stretching/compressing were suggested in the literature [27, 28]: (i) composite volume expansion, (ii) reorientation of fillers and (iii) changes in the percolation threshold. The first mechanism refers to the change of volume experienced by compressible materials subjected to strain. Given that CNTs are much stiffer than the matrix, these volume changes of fillers induced by an applied strain can be neglected, being only sustained by the matrix. Hence, a change in the overall volume with an unaltered volume of fillers induces changes in the CNT volume fraction [27, 29, 30]. This change eventually causes the breakdown of existing conductive paths or the formation of new ones due to the change of the distance between CNTs. With regard to the second mechanism, experiments have shown that CNTs tend to re-orient in the direction of the stretching [31–33]. Under the assumption of initial random distributions of CNTs, strain induced orientation changes result in a growing anisotropy and, consequently, in changes in the effective electrical properties of the composite. Finally, many researchers agree that strain induced orientation also influences the percolation threshold. This is due to the fact that aligned fillers presumably have less likelihood to get in contact and form connecting networks [34–36].

In the literature, most studies to date have focused on the fabrication and experimental analysis of CNT-based composites. In the light of the promising potential of these composites as smart materials, much effort has been put into the experimental characterization and the development of new applications as sensors [3, 4, 37–43]. Regarding the design and optimization of CNT-based composites, the theoretical understanding of the electrical conductivity is therefore imperative. However, only a very scant number of studies has faced the prediction of the electrical behavior and stretching effects. Among these contributions, some studies have proposed the application of lumped-circuit models of carbon fiber cement paste sensors based on series-parallel arrays of electrical resistors [9, 13, 44, 45] and capacitors [46]. Alternatively, micromechanics based models are attracting much attention as they allow to distinguish the contribution of electron hopping and conductive networking to the overall conductivity. A special attention should be devoted to the works of Deng and Zheng [47] and Takeda et al. [48] who employed a simplified micromechanics model to evaluate the effective electrical conductivity of CNT/polymer composites. This approach allowed to simulate percolation, conductive networks, conductivity anisotropy and waviness of CNTs with fairly good agreements with some experimental data in the literature. Another relevant contribution was made by Seidel and Lagoudas [49] and later extended by Feng and Jiang [50] who proposed a Mori-Tanaka micromechanics model [51, 52] for the study of the individual influence of electron hopping and the formation of conductive networks on the electrical conductivity of CNT-polymer composites. In that work, the electron hopping mechanism was simulated by means of a conductive interphase surrounding the tubes, whilst conductive networks were represented by changes of the CNT aspect ratios. In regards to the simulation of the stretching effects on the conductivity, the number of literature works is even more limited. The work of Lin et al. [34] is worth noting, as it presented an application of the Monte Carlo method to investigate the stretching/compression effects on the electrical properties of fiber-filled composites. Their results showed that the deformation could shift the percolation threshold of the composites. Theodosiou and Saravanos [53] analyzed the piezoresistive response of CNTs with an atomistic model and the overall behavior of CNT-polymer composites at macroscale by a numerical CNT percolation model. That work concluded that the nanotube resistance and the tunneling effect were the dominant mechanisms of strain-sensitivity of the composites. Yasuoka et al. [54] simulated CNT-based composite strain-sensitivity by using a circuit simulator analogue to percolation network. It was shown that piezoresistivity exhibits high level of non-linearity, conclusion that well agrees with the experimental evidence. Alamusi and Hu [55] proposed a three-dimensional resistor network developed by Hu et al. [56] with Simmon's tunneling effect of CNTs [57] combined with the fiber orientation model [58]. Their conclusions highlighted that composites with CNT concentrations near the percolation threshold exhibit higher strain-sensitivity. Tallman and Wang [59] extended the analytical framework developed by Takeda et al. [48] for the piezoresistivity modeling of CNT composites subjected to arbitrary three-dimensional strains. The stretching effects on percolation threshold was simulated by an excluded volume approach [60]. The results reaffirmed the non-linear behavior of the strain-sensing capability, more critical for CNT concentrations near the percolation threshold. A similar work has been recently carried out by Feng and Jiang [27, 61]. The authors extended their previous works [50] in order to take into account the stretching effects. Despite finding gross differences in comparison to some experimental data of CNT/polymer composites with low CNT concentration, the proposed framework proved capable of qualitatively implementing the three major effects induced by stretching.

It should be remarked that most of the existing theoretical analyses about the strain-induced electrical changes

were focused on the composites with the assumption of straight conductive fillers. Nonetheless, there exists experimental evidence that most CNTs in composites present a certain degree of waviness [62–64]. The reason of this non-straightness is attributed to the large aspect ratio and low bending stiffness of CNTs. Some results can be found in the literature about the effects of waviness on the overall electrical properties of CNT nanocomposites. By assuming a simple sinusoidal shape, Yi at al. [65], Berhan and Sastry [66] and Fisher et al. [67] showed that CNT waviness induces decreases of the overall conductivity by determining a shift in the percolation threshold. Similar conclusions were reached by introducing a wavy length ratio into an extended micromechanics modeling, as reported by Deng and Zheng [47] and Takeda et al. [48]. Another crucial phenomenon characterizing CNT-based composites is the agglomeration of fillers. The majority of literature studies report large difficulties in obtaining uniform dispersions of the nano-inclusions, which results to be one of the most challenging tasks of the production of CNT-based composites. Due to the electronic configuration of tube walls and their high specific surface area which enhances van der Waals (vdW) attraction forces, nanotubes tend to form aggregates in bundles [68–70]. Although the substantial effects on the piezoresistivity of the composites were already documented in the literature, only a very limited number of contributions dealt with the theoretical prediction of this effect. In this regards, the works of Weng [71] and Yang and co-authors [72] are especially noteworthy. Their results showed that, as a consequence of the inhibition of conductive networks, clustering induces important increases in the percolation threshold. These changes apparently have important influence on the strain-sensing capability of CNT-based composites. Thereof, implementation of non-straightness and agglomeration of CNTs are essential phenomena to be included in a rigorous theoretical modeling.

This paper presents a micromechanics model to predict the piezoresistive properties of CNT cement-based nanocomposites with the consideration of waviness and non-uniform spatial distributions of nanoinclusions. The two mechanisms that contribute to the conductivity of CNT composites, namely electron hopping and conductive networks, are contemplated in the mixed micromechanics framework. The origin of the piezoresistive response of these composites is attributed to (i) strain-induced changes in the volume fraction, (ii) changes in the conductive networks due to the filler reorientation and, therefore, the percolation threshold, and finally, (iii) changes in the tunneling resistance through variation of the inter-particle distance and the height of the potential barrier. The Komoro and Makishima's stochastic method is implemented in order to evaluate the variation of the percolation threshold with respect to strain through the resulting strain-induced orientation distribution function (ODF). Moreover, a helical waviness model and a two-parameter agglomeration approach are proposed. In order to count on an experimental basis to use as benchmark to validate the analytical model, several Multi-Walled Carbon NanoTube (MWCNT) reinforced cement-based specimens are manufactured and tested. In particular, specimens of cement pastes, mortars and concretes with different concentrations of MWCNTs are prepared. The proposed analytical micromechanics model is envisaged to be a helpful tool for understanding of the physical mechanisms that govern the piezoresistivity of MWCNT cement-based composites.

The paper is organized as follows. Section 2 gives a brief review of the mixed micromechanics modeling of composites doped with randomly oriented straight CNTs, as well as a helical approach for the modeling of curved CNTs, and a two-parameter model for the simulation of the agglomeration in bundles. Section 3 presents, on the basis of the previous mixed micromechanics model, the strain-induced changes that provoke the piezoresistive behavior of CNT reinforced cement-based composites. Section 3 describes the manufacturing of the tested specimens, provides detailed parametric analysis of the different variables affecting the homogenization as well as comparison against the experimental data. Section 5 concludes the paper.

2. Micromechanics modeling of cement-matrix composites with CNTs

This section introduces the micromechanics framework considered in this paper and reviews the major aspects of the model recently proposed by the authors in [73].

2.1. Composites reinforced with randomly oriented straight CNTs

Let us consider a two-phase composite consisting of a cementitious matrix doped with a volume fraction f of straight and randomly oriented CNTs, as shown in the representative volume element (RVE) in Fig. 1. A RVE designates a macroscopic point in the composite that is representative for the microstructure of the material, thus a sufficient number of fillers are considered within the RVE so that the overall properties of the composite are statistically represented. Mean-field homogenization techniques are largely employed to estimate the effective properties of a heterogeneous RVE. In particular, in the present work we use the electrical counterpart of the mean-field homogenization model of Eshelby-Mori-Tanaka. The Mori-Tanaka method [51] allows the extension of the single inclusion Eshelby's problem [74, 75] to the case of multiple inhomogeneities embedded in a finite domain. For its implementation, the orientation of every straight filler aligned in the local x_1 direction is defined by two Euler angles, φ and ψ. By means of the noninteracting inclusions assumption of the Mori-Tanaka method,

the overall electrical conductivity of the RVE can be estimated by averaging over all possible orientations of the fillers as follows [76]:

$$\boldsymbol{\sigma}_{eff} = \boldsymbol{\sigma}_m + f_{eff} \frac{\int_0^{2\pi} \int_0^{\pi} p(\varphi,\psi)\,(\boldsymbol{\sigma}_{cnt} - \boldsymbol{\sigma}_m)\,\boldsymbol{A} \sin\varphi \mathrm{d}\varphi\mathrm{d}\psi}{\int_0^{2\pi} \int_0^{\pi} p(\varphi,\psi) \sin\varphi \mathrm{d}\varphi\mathrm{d}\psi} \tag{1}$$

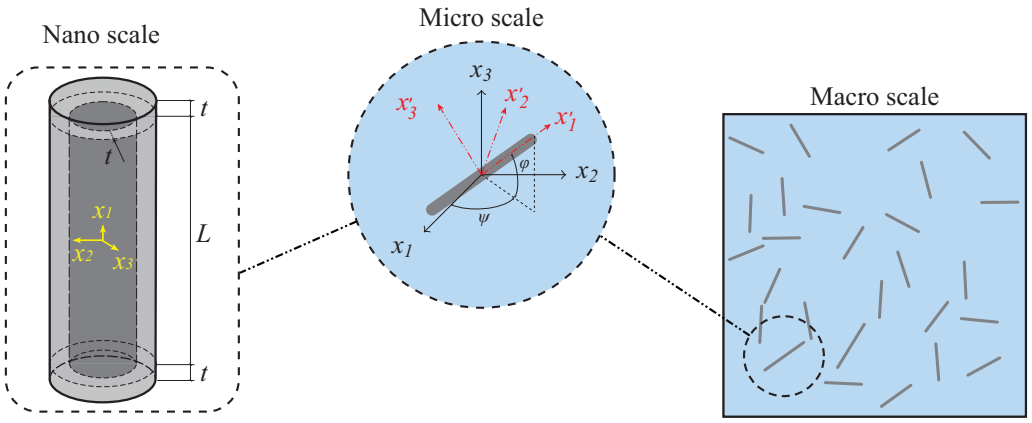

Figure 1: Representative volume element (RVE) including straight CNTs.

where $p(\varphi,\psi)$ is the orientation distribution function (ODF), f_{eff} is the effective volume fraction of the equivalent filler, and $\boldsymbol{\sigma}_{cnt}$ and $\boldsymbol{\sigma}_m$ are the electrical conductivity tensors of the effective filler and the matrix, respectively. The electric field concentration tensor, $\boldsymbol{A}$, can be expressed in the global coordinate system as [50]

$$\boldsymbol{A} = \boldsymbol{Q}^T \tilde{\boldsymbol{T}} \boldsymbol{Q} \left\{ \left(1 - f_{eff}\right) \boldsymbol{I} + f_{eff} \frac{\int_0^{2\pi} \int_0^{\pi} \left\{\boldsymbol{Q}^T \tilde{\boldsymbol{T}} \boldsymbol{Q}\right\} p(\varphi,\psi) \sin\varphi \mathrm{d}\varphi\mathrm{d}\psi}{\int_0^{2\pi} \int_0^{\pi} p(\varphi,\psi) \sin\varphi \mathrm{d}\varphi\mathrm{d}\psi} \right\}^{-1} \tag{2}$$

where

$$\tilde{\boldsymbol{T}} = \left\{ \boldsymbol{I} + \boldsymbol{S} \left(\boldsymbol{\sigma}_m\right)^{-1} \left(\tilde{\boldsymbol{\sigma}} - \boldsymbol{\sigma}_m\right) \right\}^{-1} \tag{3}$$

with $\boldsymbol{I}$ and $\boldsymbol{S}$ being the second-order identity tensor and the Eshelby tensor of the effective filler, respectively. The Eshelby tensor of a prolate spheroid ($a_2 = a_3 < a_1$) aligned in the x_1 direction is given by [77]

$$\boldsymbol{S} = \begin{bmatrix} S_{11} & 0 & 0 \\ 0 & S_{22} & 0 \\ 0 & 0 & S_{33} \end{bmatrix} \tag{4}$$

$$S_{22} = S_{33} = \frac{A_{re}}{2\left(A_{re}^2 - 1\right)^{3/2}} \left[A_{re} \left(A_{re}^2 - 1\right)^{1/2} - \cosh^{-1} A_{re} \right] \tag{5a}$$

$$S_{11} = 1 - 2S_{22} \tag{5b}$$

with A_{re} being the aspect ratio of the effective filler, i.e., A_{re}=$(L + 2t)/(D + 2t)$.

As previously discussed, the electrical conductivity of composites reinforced by CNTs is governed by two distinct mechanisms sketched in Fig. 2: electron hopping and conductive networks. The first mechanism is characterized by a quantum tunneling effect through which electrons can be transferred between proximate tubes. This effect can be included in the micromechanics model through a conducting interphase surrounding the CNTs forming an equivalent solid cylinder [49, 50]. The cut-off distance for tunneling effects, that is, the maximum possible separation between two adjacent CNTs within the cementitious matrix that permits the tunneling penetration of electrons, is taken as d_c=0.5nm as reported by Wen and Chung [78]. For a CNT volume fraction f below the percolation threshold f_c, CNTs are electrically independent and the overall conductivity of the composite is controlled by electron hopping. In this situation, the average separation distance between CNTs without electrical contacts d_a is expected to be larger than d_c, however, due to a lack of information in the literature about the estimation of this distance, it is assumed that $d_a = d_c$ [50]. Once the CNTs volume fraction reaches the percolation threshold, the CNTs begin to form conductive networks and the overall electrical conductivity is controlled by both mechanisms

simultaneously. Several works in the literature have demonstrated that the average separation distance d_a between adjacent CNTs for volume fractions above the percolation threshold ($f \geq f_c$) follows a power-law description [48, 50, 79]. In this work, we employ the expressions proposed by Deng and Zheng [47]

$$d_a = \begin{cases} d_c & 0 \leq f < f_c \\ d_c \left(\dfrac{fc}{f}\right)^{1/3} & f_c \leq f \leq 1 \end{cases} \tag{6}$$

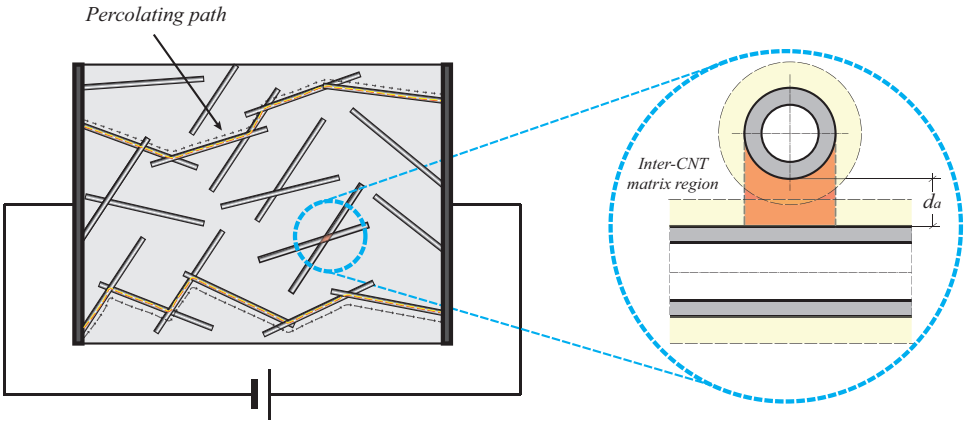

Figure 2: Schematic representation of the contribution of electron hopping and conductive network mechanisms to the overall electrical conductivity of CNT nanocomposites.

The electrical resistance of the interphase can be estimated by the generalized formula of Simmons [80] as follows

$$R_{int}(d_a) = \frac{d_a \hbar^2}{ae^2 \left(2m\lambda^{1/2}\right)} \exp\left(\frac{4\pi d_a}{\hbar} \left(2m\lambda\right)^{1/2}\right) \tag{7}$$

with m and e being the mass and the electric charge of an electron, respectively; λ the height of the tunneling potential barrier; a the contact area of the CNTs and $\hbar$ the reduced Planck's constant. The height of the potential barrier λ is taken as 0.36eV as reported by Wen and Chung [78]. Hence, the thickness and the electrical conductivity of the interphase surrounding a CNT can be obtained by

$$t = \frac{1}{2} d_a \tag{8}$$

$$\sigma_{int} = \frac{d_a}{a R_{int}(d_a)} \tag{9}$$

The equivalent composite cylinder assemblage consists of a CNT (length L and diameter $D = 2r_c$) and the surrounding interphase of thickness t. The transversely isotropic electrical conductivity tensor of the equivalent solid cylinder, $\boldsymbol{\sigma}_{cnt}$, is defined by the effective longitudinal and transverse electrical conductivity of the equivalent cylinder, $\tilde{\sigma}^L$ and $\tilde{\sigma}^T$, respectively, which can be computed by applying the Maxwell's equations and the law-of-mixture rule as [50, 81]:

$$\tilde{\sigma}^L = \frac{(L+2t)\sigma_{int}\left[\sigma_c^L r_c^2 + \sigma_{int}\left(2r_c t + t^2\right)\right]}{2\sigma_c^L r_c^2 t + 2\sigma_{int}\left(2r_c t + t^2\right) t + \sigma_{int} L \left(r_c + t\right)^2} \tag{10a}$$

$$\tilde{\sigma}^T = \frac{\sigma_{int}}{L+2t}\left[L\frac{2r_c^2\sigma_c^T + \left(\sigma_c^T + \sigma_{int}\right)\left(t^2 + 2r_c t\right)}{2r_c^2\sigma_{int} + \left(\sigma_c^T + \sigma_{int}\right)\left(t^2 + 2r_c t\right)} + 2t\right] \tag{10b}$$

The volume fraction f_{eff} of the effective solid fillers can be obtained in terms of the volume fraction of CNTs f in the matrix by

$$f_{eff} = \frac{\left(r_c + t\right)^2 \left(L + 2t\right)}{r_c^2 L} f \tag{11}$$

As mentioned before, there are some experimental and theoretical evidences that confirm the percolation-like behavior of CNT-cement nanocomposites. This behavior is characterized by a sharp rise in the electrical conductivity when CNT volume fraction reaches the percolation threshold f_c. This hasty increment of the electrical conductivity is due to the onset of the conductive network mechanism. For CNT volume fractions below this critical value, $f < f_c$, electron hopping controls the overall conductivity of the composite and the fraction of percolated CNTs, ξ, is null. Nonetheless, once percolation starts, $f = f_c$, a rising number of CNTs begin forming conductive networks. Hence, above percolation, there is a fraction ξ of CNTs that are connected forming conductive paths whilst the rest, $1 - \xi$, are still contributing solely by means of electron hopping mechanism. As reported by Deng and Zheng [47], the fraction of percolated CNTs, ξ, can be approximately estimated as

$$\xi = \begin{cases} 0 & 0 \leq f < f_c \\ \dfrac{f^{1/3} - f_c^{1/3}}{1 - f_c^{1/3}} & f_c \leq f \leq 1 \end{cases} \tag{12}$$

From the derivation above, it follows that the expression of the overall electrical conductivity of CNT-cement nanocomposites, Eq. (1), can be extended by taking into account the sum of both mechanisms as follows

$$\begin{aligned} \boldsymbol{\sigma}_{eff} =& \boldsymbol{\sigma}_m + (1-\xi)\frac{\int_0^{2\pi}\int_0^{\pi}\left\{f_{eff}\left(\boldsymbol{\sigma}_{EH} - \boldsymbol{\sigma}_m\right)\boldsymbol{A}_{EH}\right\}p(\varphi,\psi)\sin\varphi \mathrm{d}\varphi\mathrm{d}\psi}{\int_0^{2\pi}\int_0^{\pi}p(\varphi,\psi)\sin\varphi\mathrm{d}\varphi\mathrm{d}\psi} + \\ &+ \xi\frac{\int_0^{2\pi}\int_0^{\pi}\left\{f_{eff}\left(\boldsymbol{\sigma}_{CN} - \boldsymbol{\sigma}_m\right)\boldsymbol{A}_{CN}\right\}p(\varphi,\psi)\sin\varphi \mathrm{d}\varphi\mathrm{d}\psi}{\int_0^{2\pi}\int_0^{\pi}p(\varphi,\psi)\sin\varphi\mathrm{d}\varphi\mathrm{d}\psi} \end{aligned} \tag{13}$$

where subscripts EH and CN refer to electron hopping and conductive network mechanisms, respectively. In the case of CNTs forming conductive networks, several fibers are electrically connected in a continuous conductive path. This effect can be modeled by considering an infinite aspect ratio of the fibers as proposed by Seidel and Lagoudas [49]. As a result, the quantities associated with the electron hopping mechanism are defined with the real CNTs aspect ratio ($a_2 = a_3 = r_c, \quad a_1 = L$), while quantities corresponding to conductive networks are defined with an infinite aspect ratio ($a_2 = a_3 = r_c, \quad a_1 \to \infty$).

2.2. Composites reinforced with randomly oriented curved CNTs

It has been extensively reported in the literature that CNTs within cement-based composites exhibit wavy configurations. This is due to the very low bending stiffness of CNTs which have tube diameters from 10 to 15 nm. On the basis of scanning electron microscope (SEM) inspections, it is usually observed that the geometry of curved CNTs can be approximately modeled with a helical geometry. Fig. 3 shows the parametrization of these curves which are defined by the diameter D_h, the spiral angle θ and the polar angle δ. The length L_{CNT}^{wavy} of the curved CNT is defined by these parameters as:

$$L_{CNT}^{wavy} = \frac{\delta D_h}{2\cos\theta} \tag{14}$$

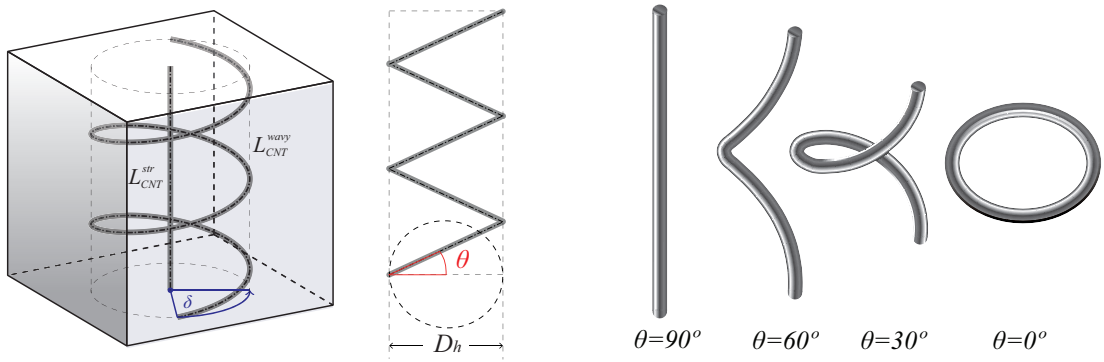

Figure 3: Helical model of a curved CNT and its equivalent straight counterpart.

The waviness of the CNTs is governed by the spiral angle, θ. Fig. 3 shows the different geometries of CNTs that can be modeled with this approach. For instance, $\theta = \pi/2$ corresponds to a straight configuration, while

$\theta = 0$ corresponds to a circular CNT. The consideration of the waviness effect into the micromechanics modeling of the conductivity of the composite requires the conversion of the wavy CNTs into straight fillers of length L_{cnt}^{str} [47, 48, 82]. A wavy CNT can be regarded as an equivalent straight fiber with the capability of (i) conducting the same electric flux J; and (ii) transporting the same amount of electric charges [50]. These conditions impose equal diameters for the wavy and the straight fillers, $D^{str} = D^{wavy}$. Finally, due to the reduction of the CNTs length from L_{cnt}^{wavy} to L_{cnt}^{str}, the volume fraction of the fillers must be updated to $f_{CNT}^{str} = \alpha f_{CNT}^{wavy}$, with f_{CNT}^{wavy} being the volume fraction of the wavy CNTs and $\alpha = L_{cnt}^{str}/L_{cnt}^{wavy} = \sin\theta$ the length ratio.

2.3. Agglomeration of CNTs: Two-parameter model for agglomeration

A second important phenomenon that must be taken into account in the modeling of CNT reinforced nanocomposites is the tendency of nanoinclusions to agglomerate in clusters. The large surface area of CNTs promotes the appearance of substantial van der Waals' attraction forces what makes CNTs easy to agglomerate in bundles [62, 83]. This effect originates spatially-inhomogeneous distributions of nano-inclusions with some local regions exhibiting higher concentrations of CNTs than the average in the composite. SEM inspections typically reveal the presence of certain regions of agglomerated fibers whose geometry can be approximately defined as ellipsoidal. In order to include the clustering effect in the micromechanics modeling approach, the bundles are assumed as ellipsoidal inclusions ($a_2 = a_3 \neq a_1$) with different conductive properties from the surrounding material (see Fig. 4). For this purpose, the two parameter agglomeration model proposed by Shi et al. [84] is here extended to model the conductivity of cement composites reinforced by inhomogeneous distributions of CNTs. The total volume V_r of CNTs in the RVE is divided into the following two parts:

$$V_r = V_r^{bundles} + V_r^m \tag{15}$$

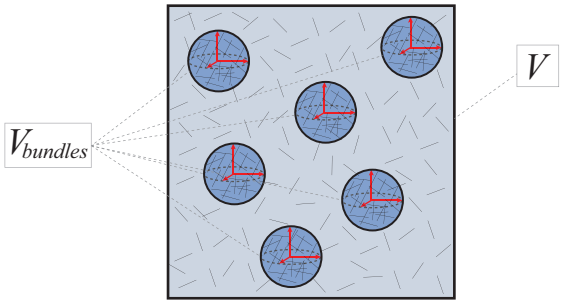

Figure 4: Sketch of RVE with ellipsoidal bundles of CNTs.

with $V_r^{bundles}$ and V_r^m being the volumes of CNTs agglomerated in the bundles and dispersed in the matrix, respectively. In order to characterize the clustering, two agglomeration parameters χ and ζ are introduced as:

$$\chi = \frac{V_{bundles}}{V}, \quad \zeta = \frac{V_r^{bundles}}{V_r} \tag{16}$$

where $V_{bundles}$ is the volume of ellipsoidal bundles in the RVE, and χ the volume ratio of the bundles with respect to the total volume V of the RVE (Fig. 4). When χ=1 CNTs are uniformly dispersed in the matrix, whilst the less χ the more inhomogeneous distribution of nano-inclusions. Parameter ζ stands for the volume ratio of nanotubes that are dispersed in bundles with respect to the total volume of nanotubes. The limit case of ζ=1 represents the state in which all the nanotubes are agglomerated in bundles. On the contrary, perfect uniform distributions of CNTs lead to χ=ζ. The effect of the variation of these two parameters are depicted in Fig. 4. The Eshelby's tensor for an ellipsoid inclusion with x_1 the axis of symmetry ($a_2 = a_3 \neq a_1$) is given by:

$$S_{22} = S_{33} = \begin{cases} \dfrac{\alpha}{2\left(\alpha^2 - 1\right)^{3/2}}\left[\alpha\left(\alpha^2 - 1^{1/2}\right) - \cosh^{-1}\alpha\right]; & \alpha \geq 1 \\ \dfrac{\alpha}{2\left(\alpha^2 - 1\right)^{3/2}}\left[cos^{-1}\alpha - \alpha\left(1 - \alpha^2\right)^{1/2}\right]; & \alpha \geq 1 \end{cases} \tag{17}$$

with α being the aspect ratio of the ellipsoid (a_1/a_2) and S_{11}=$1 - 2S_{22}$.

3. Micromechanics modeling of piezoresistivity of cement-matrix composites with CNTs

In this section, a micromechanics modeling of the piezoresistivity of CNT reinforced cement-matrix composites is developed as an extension of the previously described approach. The origin of the strain sensing capabilities of the cement-based nanocomposites is attributed to three main mechanisms: (i) volume expansion and reorientation of CNTs, (ii) changes in the conductive networks, and (iii) changes in the tunneling resistance. The following sections separately present the modeling approach for each of these contributions.

3.1. Volume expansion and reorientation of CNTs

Let us consider a three-dimensional affine deformation cell containing an embedded effective solid filler before and after the application of a uniaxial strain ϵ as shown in Fig. 5. Under the assumption of small deformations, the volume of the cell changes from $V_o = l_o^3$ to $V = l_o^3 (1+\epsilon)^{1-2\nu}$, with ν being the Poisson's ratio of the composite. Moreover, assuming that the deformation of the composite is mainly sustained by the matrix, the volume of the nano-inclusions remains constant and, therefore, the volume expansion induces changes in the CNT volume fraction as follows [27]:

$$f^* = \frac{V_o f}{V} = \frac{f}{(1+\epsilon)^{1-2\nu}} \tag{18}$$

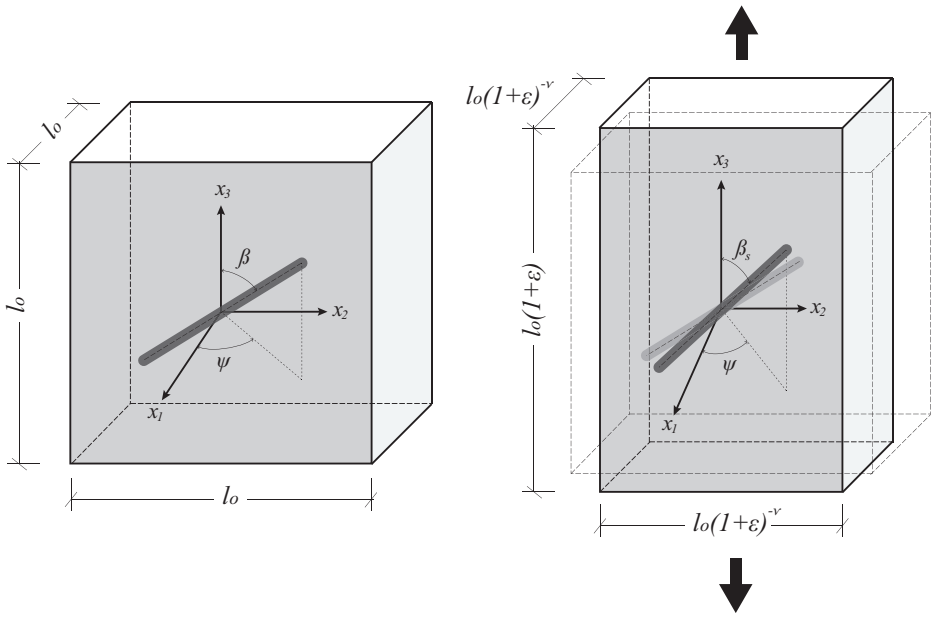

Figure 5: Schematic representation of the volume expansion and reorientation of a conductive filler within a deformable cell subjected to uni-axial strain ϵ.

Likewise, it can be noted from Fig. 5 that the strain ϵ also originates a re-alignment of the fiber along the strain direction x_3. This change of orientation is characterized by a decrease in the polar angle from β to β_s, with negligible variation of the azimuth angle ψ [27]. The new polar angle β_s can be expressed in terms of its initial value β as follows [58]:

$$\tan\beta_s = (1+\epsilon)^{1+\nu} \tan\beta \tag{19}$$

This change of the polar angle of the fillers results in a change of the ODF from $p(\psi,\beta)$ to $p(\psi,\beta_s)$. After the application of the strain, the initially randomly distributed fillers ($p(\psi,\beta) = 1$) tend to align in the strain direction and, therefore, the randomness of the nanofillers distribution is reduced. In order to obtain the resulting ODF, the condition of a constant number of fillers before and after the application of the strain has been applied. To this end, and assuming a total number of G fillers distributed in the RVE, the number of fillers lying in the orientation range $(\beta,\beta+\mathrm{d}\beta)\times(\psi,\psi+\mathrm{d}\psi)$ can be computed as [27]:

$$\mathrm{d}N_{\substack{\beta,\beta+\mathrm{d}\beta \\ \psi,\psi+\mathrm{d}\psi}} = \frac{1}{\pi} G p(\psi,\beta) \sin\beta \mathrm{d}\beta \mathrm{d}\psi \tag{20}$$

Accordingly, the total number of fillers must be the same after the application of the strain within the range $(\beta_s, \beta_s + \mathrm{d}\beta_s) \times (\psi, \psi + \mathrm{d}\psi)$:

$$\mathrm{d}N_{\substack{\beta_s,\beta_s+\mathrm{d}\beta_s \\ \psi,\psi+\mathrm{d}\psi}} = \mathrm{d}N_{\substack{\beta,\beta+\mathrm{d}\beta \\ \psi,\psi+\mathrm{d}\psi}} \tag{21}$$

Substituting Eq. (19) into Eq. (21), and expressing ψ as $\pi/2 - \beta$ (see Fig. 5), the resulting ODF, $p(\varphi, \psi)$, is determined as:

$$p(\varphi, \pi/2 - \beta) = \frac{(1+\epsilon)^{\frac{1+\nu}{2}}}{\left[(1+\epsilon)^{-(1+\nu)} \cos^2(\pi/2-\beta) + (1+\epsilon)^{(1+\nu)} \sin^2(\pi/2-\beta)\right]^{\frac{3}{2}}} \tag{22}$$

Fig. 6 shows the variation of the ODF with the strain ϵ and the polar angle β. In the unloaded case, $\epsilon = 0$, the ODF remains constant and equal to 1 for every polar angle, corresponding to the uniform random distribution. It is also observed that, for increasing traction ($\epsilon > 0$), the ODF gives more weight to polar angles close to 0 and π, i.e., more fibers tend to re-align in the direction of the strain. On the contrary, it is worth noting that for increasing compression ($\epsilon < 0$), the ODF has higher values for polar angles around $\pi/2$ and, therefore, the fibers tend to re-align in the transverse direction of the strain.

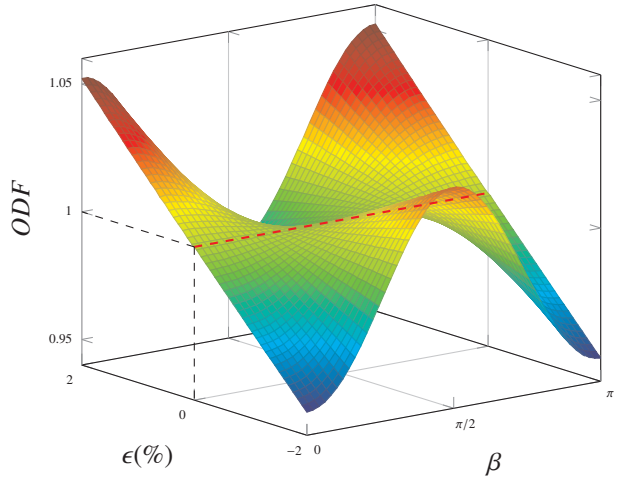

Figure 6: Variation of $p(\varphi, \psi)$ (ODF) with strain ϵ and polar angle β ($\nu = 0.3$).

3.2. Change in the conductive networks

Piezoresistivity of CNT nanocomposites is also due to the breakage of conductive networks induced by strain. As previously discussed, the reorientation of the fibers decreases the randomness of the CNT distribution as the strain increases. Hence, it can be intuitively understood that the probability of forming conductive paths must be altered, which corresponds to the change in the percolation threshold f_c. According to the definition of the orientation distribution function $p(\varphi, \psi)$, the probability of finding a nanotube lying in an infinitesimal range of angles $[\varphi, \varphi + \mathrm{d}\varphi,] \times [\psi, \psi + \mathrm{d}\psi,]$ is given by $p(\varphi, \psi) \sin\varphi \mathrm{d}\varphi \mathrm{d}\psi$, which satisfies the normalization condition:

$$\int_0^{\pi} \mathrm{d}\varphi \int_0^{\pi} p(\varphi, \psi) \sin\varphi \mathrm{d}\psi = 1 \tag{23}$$

Komoro and Makishima [85] proposed a stochastic approach for the calculation of the number of filler contacts in general disordered systems coped with rod-like inclusions with constant length and diameter. According to that work, a filler A with a given orientation (φ, ψ) comes into contact with a second filler B with orientation (φ', ψ') if the center of mass of the former is located within the neighbourhood region of the latter. The neighbourhood region is defined when the fiber B is slid over both sides of the fiber A from one end to the other, keeping the direction and the contact point on B unchanged (see Fig. 7). In these two sweepings, the axis of B makes two rhombuses near both sides of A, conforming a parallelepiped. The volume of this region is $V = 2DL^2 \sin\tau$, with τ being the angle between the two nanofillers. Based on the defined number of contacts in a volume V along with the probability of formation of a contact, the mean distance among contacts, $\bar{b}_{KM}$, is given by:

$$\bar{b}_{KM} = \frac{\pi D}{8If} \tag{24}$$

where

$$I = \int_0^{\pi} \mathrm{d}\varphi \int_0^{\pi} J(\varphi, \psi) \sin\varphi \mathrm{d}\psi \tag{25}$$

$$J(\varphi, \psi) = \int_0^{\pi} \mathrm{d}\varphi' \int_0^{\pi} \sin\tau(\varphi, \psi, \varphi', \psi') p(\varphi', \psi') \sin\varphi \mathrm{d}\psi' \tag{26}$$

$$\sin\tau = \left[1 - \{\cos\varphi\cos\psi + \cos(\psi - \psi')\sin\varphi\}^2\right]^{1/2} \tag{27}$$

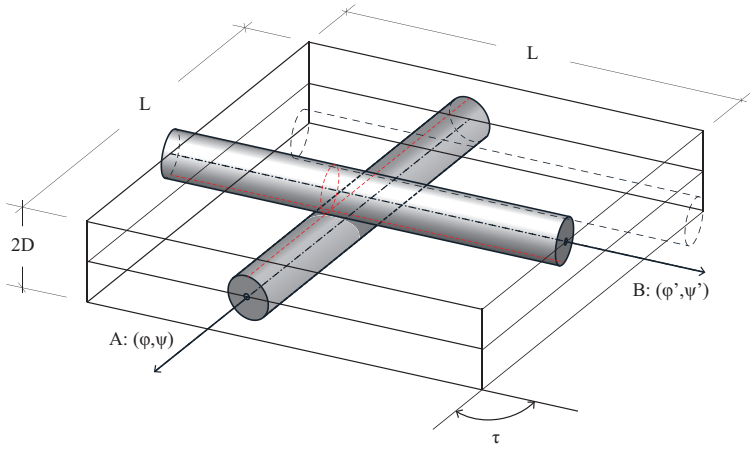

Figure 7: Neighbourhood of the contact region of a fiber A of orientation (φ, ψ) defined by the parallelepiped formed by a second fiber B of orientation (φ', ψ') sliding over both sides of the former.

It should be mentioned that Komoro and Makishima did not consider the changes in the contact probability with successive contacts. Pan [86] reported about this issue and proposed an extended approach by considering that an existing contact reduces the effective contact length of a filler, which reduces the probability of forming a new contact. A new expression of the mean distance among inclusions $\overline{b}_{Pan}$ was given as:

$$\overline{b}_{Pan} = \frac{(\pi + 4f\eta)D}{8fI} \tag{28}$$

where

$$\eta = \int_0^{\pi} \mathrm{d}\varphi \int_0^{\pi} J(\varphi, \psi) K(\varphi, \psi) \sin\varphi \mathrm{d}\psi \tag{29}$$

$$K(\varphi, \psi) = \int_0^{\pi} \mathrm{d}\varphi' \int_0^{\pi} \frac{p(\varphi', \psi')\sin\varphi'}{\sin\tau(\varphi, \psi, \varphi', \psi')} \mathrm{d}\psi' \tag{30}$$

Finally, it is worth noting that each nanofiller must have at least two contact points to be part of a conductive network in the nanocomposite [87]. Alternatively, the mean distance between contacts should be at least half of the filler length to attain the percolation threshold. Kumar and Rawal [88] defined a coverage parameter, $\Gamma = b/L$, which represents the number of contacts formed on a given filler length, so that for percolated nanofillers this quantity is such that $\Gamma \leq 0.5$. Moreover, those authors also proposed a mean coverage parameter, $\overline{\Gamma} = \overline{b}/L$, as the probability of percolation of the composite. Furthermore, it has been reported in the literature that the distance between the contacts exhibit an exponential distribution [89, 90], and similarly, the mean coverage parameter $\overline{\Gamma}$ can be defined as[88]:

$$P(\Gamma) = (1/\overline{\Gamma})\exp\left(-\Gamma/\overline{\Gamma}\right) \tag{31}$$

Zheng et al. [91] reported that the statistical percolation threshold is reached when 50% of the sample percolates, this is:

$$\int_0^{0.5} P(\Gamma)\mathrm{d}\Gamma = -\exp(0.5/\overline{\Gamma}) + 1 = 0.5 \tag{32}$$

where a value $\overline{\Gamma}$ of 0.72 is extracted. Finally, combining this result with Eqs. (25) and (28), the percolation threshold can be computed using the Komori-Makishima and Pan's models as:

$$f_c^{KM} = \frac{\pi}{5.77sI} \tag{33}$$

$$f_c^{Pan} = \frac{\pi}{5.77sI - 4\eta} \tag{34}$$

with s being the aspect ratio of the nanofillers, i.e. L/D. Kumar and Rawal [88] reported that there are only slight differences between the Komori and Makishima and Pan's models since the percolation threshold is often reached at significantly low nanofiller concentrations. Similar conclusions are also obtained in the present work and, therefore, all the results that are provided thereafter are obtained by using the Komoro and Makishima's model. This methodology has allowed us to relate the externally applied deformation with the variation of the percolation threshold through the orientation distribution function, previously defined in Eq. (22). Fig. 8 shows the variation of the percolation threshold with respect to the nanofiller aspect ratio and for different strain levels. It can be extracted from this figure that, due to the reorientation of the fillers caused by the strain, some conductive paths disappear and consequently the percolation threshold increases. In addition, Fig. 9(a) shows different orientation distribution functions for polar angles varying from 0 to π under different levels of uni-axial strain. As already discussed in the previous section, in the case of stretching ($\epsilon > 0$), the nanotubes tend to re-align in the direction of the strain, whilst in the case of compression ($\epsilon < 0$), the tendency is the opposite and the fillers tend to re-align perpendicularly to the strain. In both cases, the loss of randomness of the nanofillers distribution leads to lesser probability of forming conductive paths as it can be seen in Fig. 9(b). Hence, it can be concluded from this figure that both compression and traction lead to higher percolation thresholds.

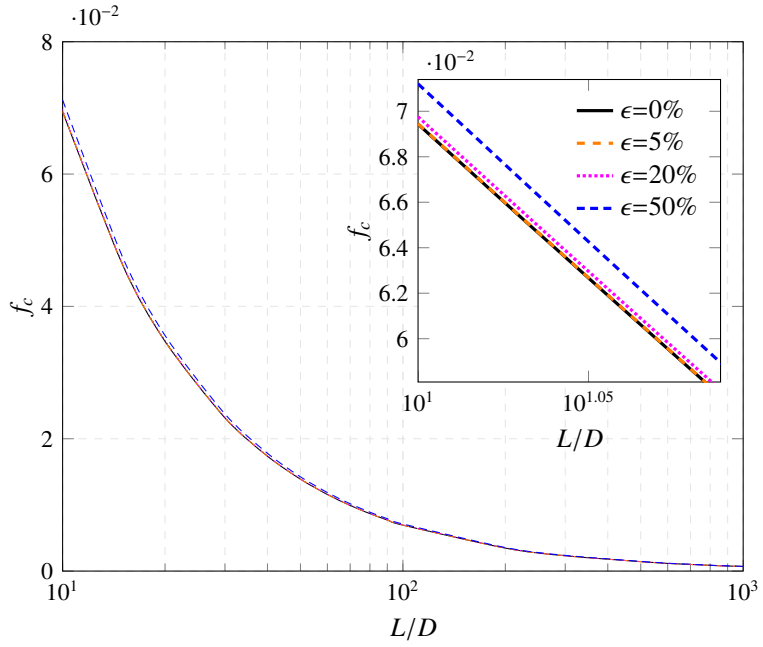

Figure 8: Percolation threshold versus CNTs volume fraction under different strain levels (ν=0.3).

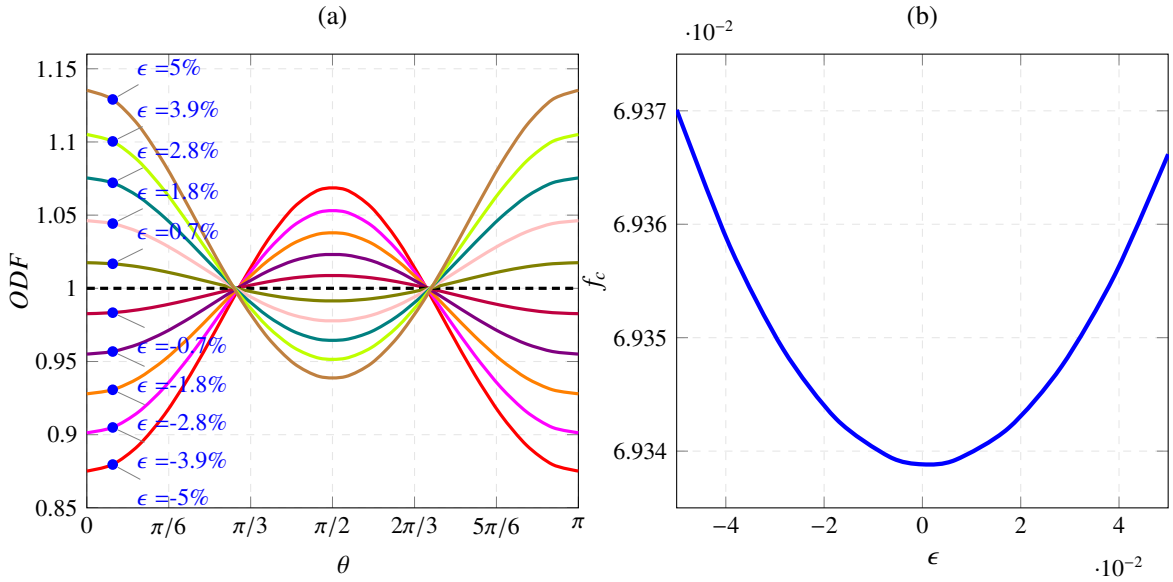

Figure 9: a) Orientation distribution functions under different strain levels, and b) variation of the percolation threshold with respect to the strain level (ν=0.3).

3.3. Change in the tunneling resistance

The third mechanism originating the strain-sensing property of the composites is related to the circumstance that electron hopping is altered when a deformation is applied because of the separation of the particles and of changes in the inter-particle distance. It has been reported in the literature that when a nanocomposite is deformed under external strain, the change of the nanotube resistance is expected to be negligible because of the extremely small elastic deformation in nanotubes resulting from their high elastic modulus while the large deformation in the inter-nanotube matrix due to its low modulus contributes to the electrical resistance change of the composite [92]. It has been also reported in the literature that, at relatively low strains ($< 10^{-4}$), the inter-particle distance and the height of the potential barrier change proportionally with the strain [93] as follows:

$$d_a = d_{a,0}(1 + C_1\epsilon) \tag{35}$$

$$\lambda = \lambda_0(1 + C_2\epsilon) \tag{36}$$

where $d_{a,0}$ and λ_0 are the initial inter-particle distance and potential height at zero strain, respectively, and C_1 and C_2 are constants. The constants C_1 and C_2 can be obtained by fitting experimental data. There still exists a lack of information in the literature about this aspect and, therefore, further future research is needed in order to develop a fully experimental independent tool for design purposes.

4. Results and discussion

In this section, the proposed analytical model is tested against experimental data from MWCNT reinforced cement-based specimens. Moreover, the influence of the different variables affecting the strain-sensitivity is also examined. In our calculations, the electrical conductivities of the three different matrices have been selected as 2.8×10^{-3} S/m, 1.04×10^{-3} S/m and 2.92×10^{-4} S/m, for cement paste (PA), cement mortar (MO) and concrete (CO), respectively [94, 95]. In order to compare the theoretical and experimental results, the resistivity of the electrodes and the contact resistance need to be properly taken into account [13]. Hence, an equivalent in series circuit with conductivity σ_{spc} is defined, in which the resistivity of the electrodes and the contact resistance are computed so that the conductivity of the initial plain configuration (f=0) is fitted. Having regard to the commercial specifications of MWCNTs (further discussed in the next section), the electrical conductivity of MWCNTs has been set in the range 10^0-10^7 S/m. The values of the constants used in Simmon's model for the evaluation of the interphase conductivity in Eq. (7) are given in Table 1. For practical convenience, the concentration f of carbon nanotubes is usually expressed in the literature in terms of mass content with respect to mass of cement, wt, as follows:

$$wt = \frac{\rho_N}{m_{cem}} f \tag{37}$$

with ρ_N being the density of the carbon nanotubes, taken as 150 kg/m^3, and m_{cem} the mass of cement in the composite.

Table 1: Physical constants used in Simmon's model

Mass of electron m	9.10938291×10^{-31} kg
Electric charge of an electron e	$-1.602176565\times10^{-19}$ C
Reduced Planck's constant $\hbar$	6.626068×10^{-34}m^{2}kg/s

4.1. Experiments

As discussed above, in order to validate the micromechanics model developed in the current work, the modeling results are compared to the experimental data obtained by testing specimens made of composite cement paste (PA), mortar (MO) and concrete (CO) doped with MWCNTs. The multi-walled carbon nanotubes utilized as filler for the cementitious matrices was type Graphistrength C100 provided by group Arkema. Their main physical, chemical and mechanical characteristics are reported in Table 2. Such type of conductive fillers have suitable electrical properties due to their peculiar aspect ratio.

Table 3 shows the mix design of the different typologies of cementitious materials, with and without carbon fillers. The cement was pozzolanic, type 42.5. Aggregates were added to obtain mortars and concretes. In particular sand with a nominal dimension between 0-4 mm and gravel with nominal dimensions between 4-8 mm were used. The water/cement ratio was 0.45 for all the mixes. A second-generation plasticizer based on polycarboxylate ether polymers was added to obtain a comparable workability for all the cementitious materials. The specimens were cubes with sides of 51 mm instrumented with five embedded stainless steel nets as electrodes, placed at a mutual distance of 10 mm (Fig. 10(a)). The nets were constituted by 0.5 mm diameter wires placed to form a mesh of 6 mm. In the case of concrete, the embedded part was resulted in wires at a mutual distance of 12 mm.

Fig. 10(b) shows concrete samples with decreasing amount of nanotubes. Fig. 10(c) presents the experimental setup of the electromechanical tests carried out using the 2-probe method using two electrodes placed at a distance of 10 mm, showing the load testing machine and the data acquisition system of the electrical measurements.

Fig. 11 sketches the preparation process for the nanomodified samples of paste, mortar and concrete. First, the dispersant (sodium lignosulfonate salt) was mix in deionized water and then the various amounts of carbon nanotubes were introduced within the solution (Fig. 11(a). The fillers were dispersed by a preliminary mechanical mixing (Fig. 11(b)) and by use of a sonicator (Fig. 11(c)). The nanomodified suspension were mixed with cement and eventually aggregates and plasticizer to achieve the different cementitious materials(Fig. 11(d)). The admixture was then poured into oiled molds, the electrodes were embedded (Fig. 11(e)) and the samples completed the curing period in controlled laboratory conditions (Fig. 11(f)). A drop of a suspension after sonication and a fragment of hardened material were analyzed by use of SEM micrographs in order to investigate the dispersion of the carbon nanotubes during and after the preparation (Fig. 11(c1) and 11(f1)). Fig. 12 shows the good dispersion obtained in the water suspensions after sonication (Fig. 12(a)) and in a hardened mortar matrix after curing (Fig. 12(b)).

The strain sensing capabilities of the cementitious composites were investigated subjected the samples to cyclic axial compression loads with increasing loads (Fig. 13(a)), by use of a servo-controlled pneumatic universal testing machine of 14kN load capacity, model IPC Global UTM14P. Fig. 13(b) is a detailed view of a samples during the setup of the mechanical tests. The strain sensing properties were investigated by measuring the current passing through two electrodes placed at a distance of 10 mm under the application of a stabilized voltage of 2.5 V. The source measure unit and the high speed digital multimeter were model NI PXI4130 and NI PXI4071 devices, respectively. Two electrical strain gauges 2 cm long, with a nominal resistance of 120 Ω and a gauge factor of about 2 were also attached at opposite faces of the specimens and acquired using a data acquisition card, model NI PXIe-4330. Strain-induced incremental variation in electrical resistance of the composites, $\Delta R(t)$, was obtained by dividing the applied voltage, V, by the incremental variation in measured current intensity, $\Delta I(t)$. Under the assumption of small strains, the correlation between the relative change in resistance, $\Delta R/R_o$, and the applied compressive strain, ϵ, can be modeled likewise conventional strain gauges as:

$$\frac{\Delta R}{R_o} = \lambda^{-}\epsilon, \quad \epsilon < 0 \tag{38}$$

where λ^{-} is the so-called gauge factor. Although only compression tests were carried out, the presented approach also allows to model tensile stresses. As further discussed in the next section, the piezoresistive behavior of CNT reinforced composites is slightly different under compressive and tensile stresses. Hence, superscripts "−" and "+" are used for gauge factors in the case of compressive ($\epsilon < 0$) and tensile ($\epsilon > 0$) strains, respectively.

Table 2: Main characteristics of MWCNTs used in the experiments (from Ref. [96])

Property	**Value**	**Property**	**Value**
Mean agglomerate size	200-500 μm	Apparent density	50-150 kg/m^3
Mean number of walls	5-15 μm	Weight loss at 105 °C	<1%
Outer mean diameter	10-15 nm	Thermal Conductivity	>3000 W/(mK)
Length	0.1-10 μm	Electric Conductivity	up to 10^7 $(\Omega m)^{-1}$
Carbon content	>90% in weight	Young Modulus	>1 TPa
Surface area	100-250 m^2/g	Tensile strength	≈ 150 GPa

Table 3: Mix designs of cementitious samples with six different concentrations of MWCNTs (the ratio ν between the mass of MWCNTs and cement varies from 0 to 1.5%). C_{0i} and C_i are the masses of cement in normal materials and with MWCNTs, respectively. ΔV_p, ΔV_m and ΔV_c are the total volumes of MWCNTs plus dispersant for paste, mortar and concrete nanomaterials, respectively, while η is the ratio between dispersant and MWCNTs, equal to 1 or to 10. [43].

Components	**Paste kg/m^3**		**Mortar kg/m^3**		**Concrete kg/m^3**	
	Normal	**With MWCNTs**	**Normal**	**With MWCNTs**	**Normal**	**With MWCNTs**
Cement pozzolanic, 42.5	C_{0p}=1277	C_p=$C_{0p}\frac{1m^3}{1m^3+\Delta V_p}$	C_{0m}=654	C_m=$C_{0m}\frac{1m^3}{1m^3+\Delta V_m}$	C_{0c}=524	C_c=$C_{0c}\frac{1m^3}{1m^3+\Delta V_c}$
Water	W_{0p}=574	0.45C_p	W_{0m}=294	0.45C_m	W_{0c}=234	0.45C_c
MWCNTs	-	νC_p	-	νC_m	-	νC_c
Dispersant	-	$\eta\nu C_p$	-	$\eta\nu C_m$	-	$\eta\nu C_c$
Sand	-	-	1308	2C_m	951	1.81C_c
Gravel	-	-	-	-	638	1.22C_c
Plasticizer	-	Var	-	Var	2.62	Var
W/C ratio	0.45	0.45	0.45	0.45	0.45	0.45

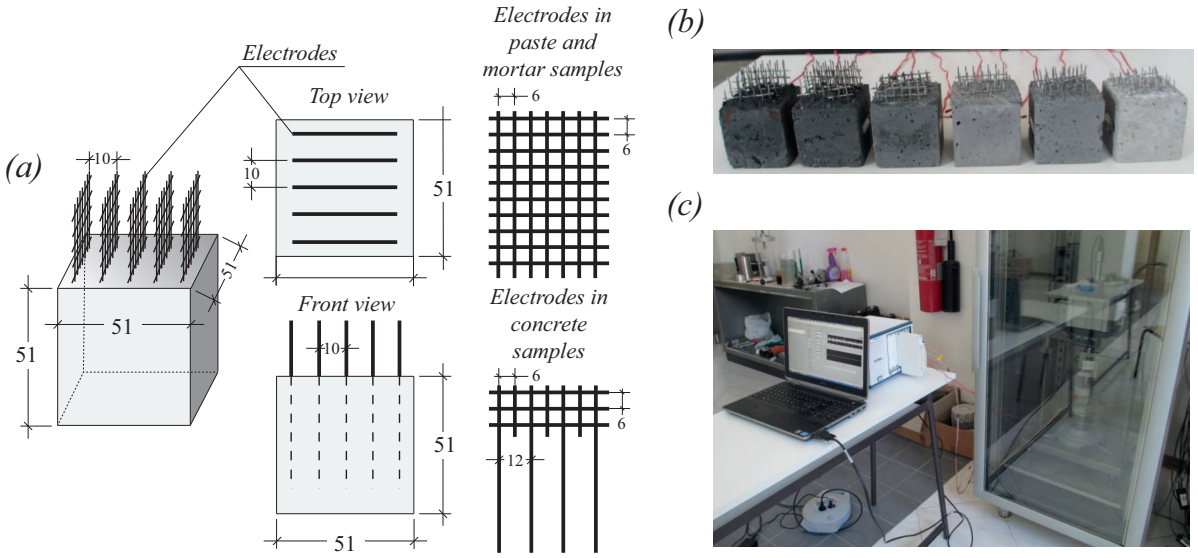

Figure 10: Geometry and dimensions of the cementitious samples and of the electrodes (a), picture of some samples with the embedded electrodes (b) and setup of the experimental electrical tests under applied axial load (c) (Units in mm).

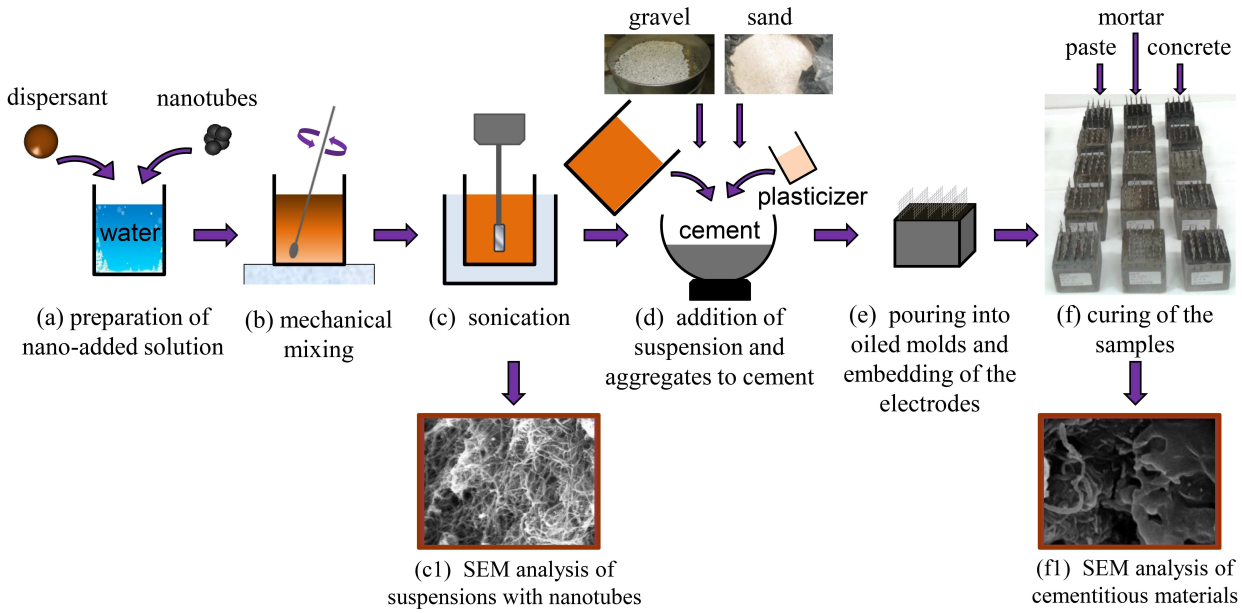

Figure 11: Preparation procedure of paste, mortar and concrete samples with MWCNTs.

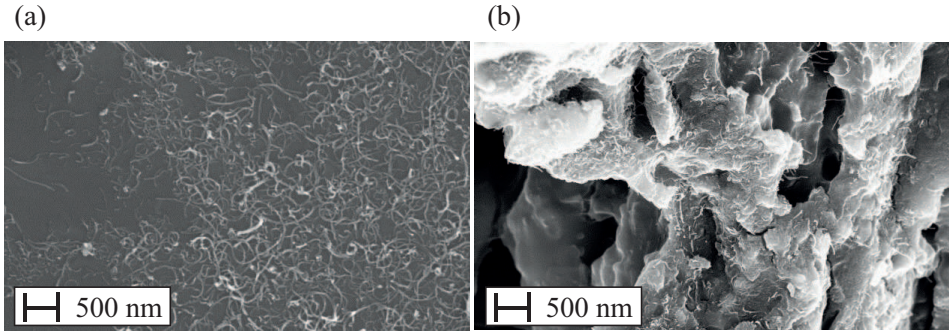

Figure 12: SEM pictures of MWCNTs dispersed in water solution (a) and in a mortar matrix (b).

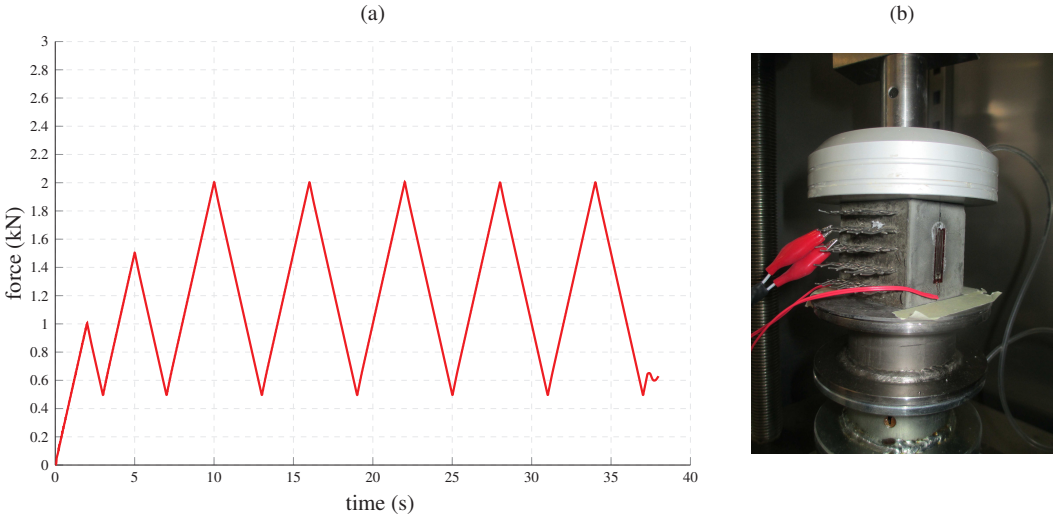

Figure 13: (a) Applied compression load and (b) uniaxial testing setup.

4.2. Parametric analyses

In this first set of analyses, detailed parametric studies have been carried out in order to give some insight into the structure of the proposed model, as well as to extract valuable conclusions for the design of self-sensing MWCNT reinforced cement-based composites.

4.2.1. Effects of constituents properties

Fig. 14 shows the relative change in resistance $\Delta R/R_o$ of MWCNT reinforced cement paste (PA) with different filler concentrations f. For illustrative purposes, the variation parameters of the inter-particle properties, C_1 and C_2, have been chosen from [93] as 8.9045 and 0.0243, respectively. According to the physical properties of cement paste, the Poisson's ratio has been set to 0.2. The externally applied strain has been imposed in the range $-1\times10^{-4}/+1\times10^{-4}$. Despite only compression tests have been carried out, theoretical results dealing with tensile strains are also shown here for the sake of completeness and potential application of this approach for stretchable materials. It can be seen that the proposed approach reproduces some of the effects evidenced in the experiments. For compressive loadings, $\epsilon < 0$, the composites exhibit higher values of conductivity, unlike for tensile strains. In both cases, the percolation threshold increases although for the considered ranges of deformation the effect of the volume expansion and variation of the inter-particle properties becomes predominant. This behavior can be also seen in Fig. 15, where the overall electric conductivity for different MWCNT concentrations and strain levels is represented. In Fig. 14(a), different MWCNT contents have been selected according to different parts of the percolation curve from Fig. 14(b). It is noticeable that for MWCNT concentrations below and above the percolation threshold, the strain-sensitivity of the composite is considerably low. On the contrary, filler concentrations close to the percolation threshold lead to the highest sensitivity values. This fact justifies the evidence from the experiments about the existence of a critical concentration where the gauge factor reaches a maximum. This maximum is obtained for filler concentrations around the percolation threshold.

In order to gain a better insight into the underlying mechanisms that control the piezoresistivity of the composites, Figs. 16(a) and (b) present the relative resistance change induced by the isolated contribution of the different mechanisms and filler concentrations of 0.965 and 1.2%, respectively. Four different cases S_i have been selected with S_1, S_2, S_3 and S_4 standing for the isolated contribution of the volume expansion, change of the percolation threshold, filler orientation and tunneling resistance, respectively. It can be seen that for the first concentration, Fig. 16(a), close to the percolation threshold, the strain sensitivity is dominated by the volume expansion (S_1). This fact makes sense since for this concentration only a few conductive paths have been formed. Thus, a change in the effective volume fraction has a deep impact as directly varies the number of formed paths. On the other hand, for filler concentrations far above the percolation threshold, Fig. 16(b), the number of conductive paths is larger and the strain sensing capability is held by the different mechanisms. In this case, the volume expansion continues being dominant although the reorientation of the fillers has gained importance. The change in the tunneling resistance has limited influence and the change of the percolation threshold has little influence. Fig. 17 represents each contribution from Fig. 16(b) separately. From this figure, it is interesting noticing that the change of the percolation threshold increases the resistance for both compressive and tensile strains, according to Fig. 9. The strain sensitivity induced by the volume expansion and change in the tunneling resistance reduces the resistance for compressive strains and vice versa. This behavior is also expected as both an increase of the volume fraction and a reduction of the inter-particle distance lead to higher values of conductivity for compressive loadings. The reasoning is the same in the case of tensile strains. Conversely, the contribution of the reorientation of the fillers exhibits an opposite behavior. As we are measuring the resistivity along the direction of the applied strain, for compressive loadings the fillers tend to align in the transverse direction reducing the measured conductivity. In the case of tensile loadings, the fillers tend to align in the direction of the load increasing the measured conductivity.

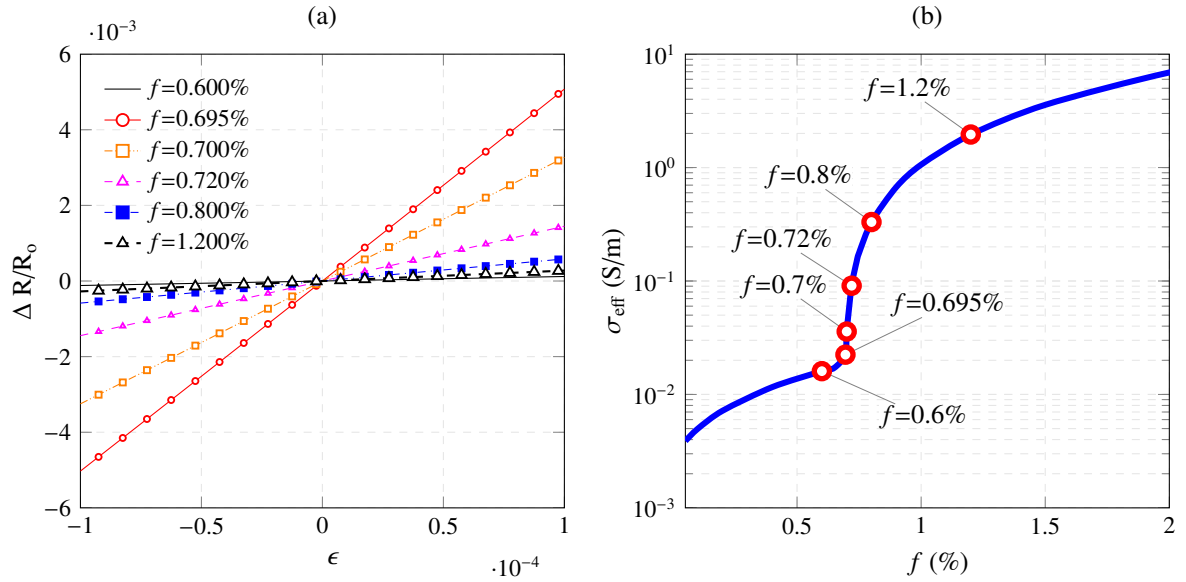

Figure 14: Strain-sensing capabilities of MWCNT reinforced cement paste with different filler concentrations (a) and unloaded overall electrical conductivity of MWCNT reinforced cement paste (PA, ν=0.2, L = 1 μm, D=10 nm, λ=0.36 eV, d_c=0.5 nm, σ_c = 10^4 S/m, C_1=8.9045, C_2=0.0243).

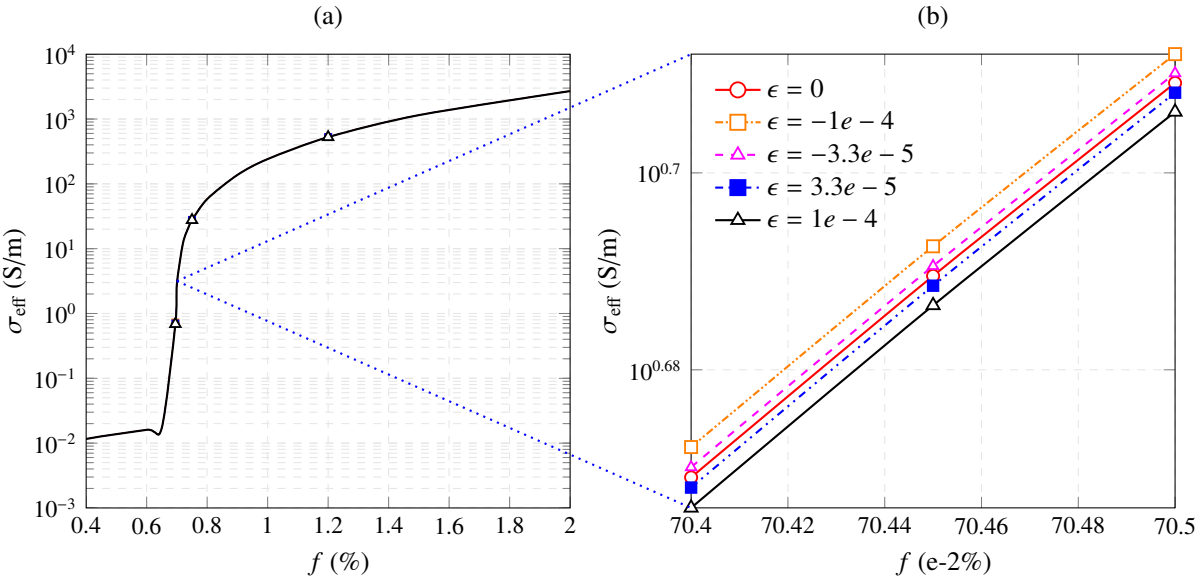

Figure 15: Overall electrical conductivity of MWCNT reinforced cement paste under different strain levels (a), and detail view (b) (PA, ν=0.2, L = 1 μm, D=10 nm, λ=0.36 eV, d_c=0.5 nm, σ_c = 10^7 S/m, C_1=8.9045, C_2=0.0243).

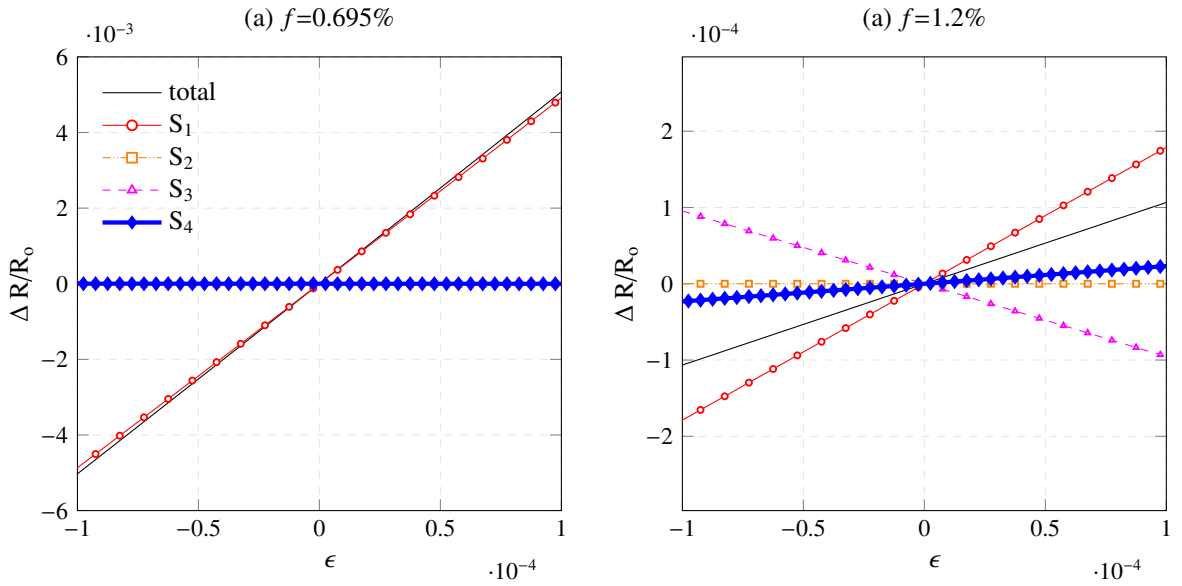

Figure 16: Piezoresistive behavior of MWCNT reinforced cement paste with isolated contributions of the strain-sensing mechanisms (S_1 volume expansion contribution, S_2 contribution of change the in the percolation threshold, S_3 effect of the fiber reorientation and, S_4 change in the tunneling resistance)(PA, ν=0.2, L = 1 μm, D=10 nm, λ=0.36 eV, d_c=0.5 nm, σ_c = 10^4 S/m, C_1=8.9045, C_2=0.0243).

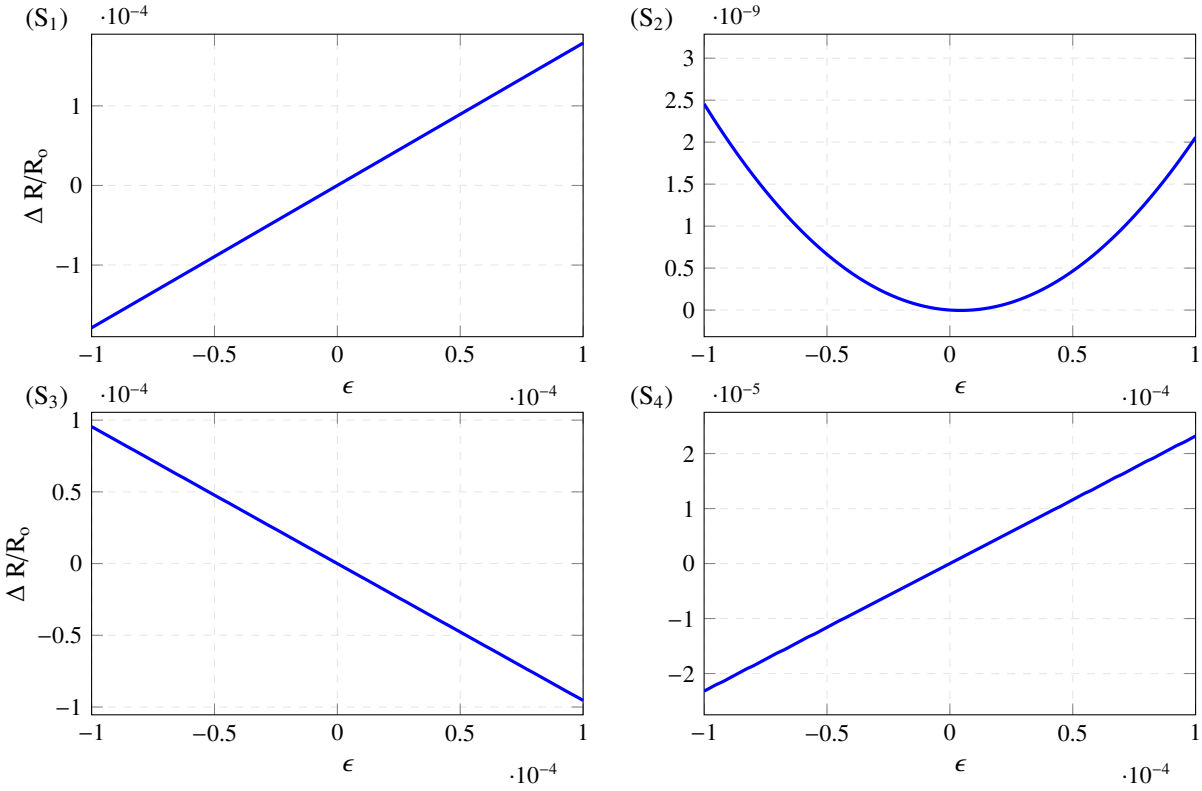

Figure 17: Isolated contributions of the strain-sensing mechanisms (S_1 volume expansion contribution, S_2 contribution of change the in the percolation threshold, S_3 effect of the fiber reorientation and, S_4 change in the tunneling resistance)(PA, ν=0.2, L = 1 μm, D=10 nm, λ=0.36 eV, d_c=0.5 nm, σ_c = 10^4 S/m, C_1=8.9045, C_2=0.0243).

Literature studies have reported about the dominant role of the tunneling-type contact resistance in the strain-sensing capabilities of CNT reinforced composites [93]. In this regard, as it can be seen in Eq. (7), the height of the potential barrier λ and the initial inter-particle distance d_c play a key-role in the electron hopping mechanism. The relative resistance change for different values of λ and d_c is presented in Figs. 18(a) and 18(b), respectively. The

MWCNT concentration has been set as f=0.695%, value that is close to the percolation threshold (see Fig. 14(b)). The results presented in these two figures show that the lesser are the values of these two variables, the higher are the strain-induced changes and, thus, the higher is the strain sensitivity of the composite.

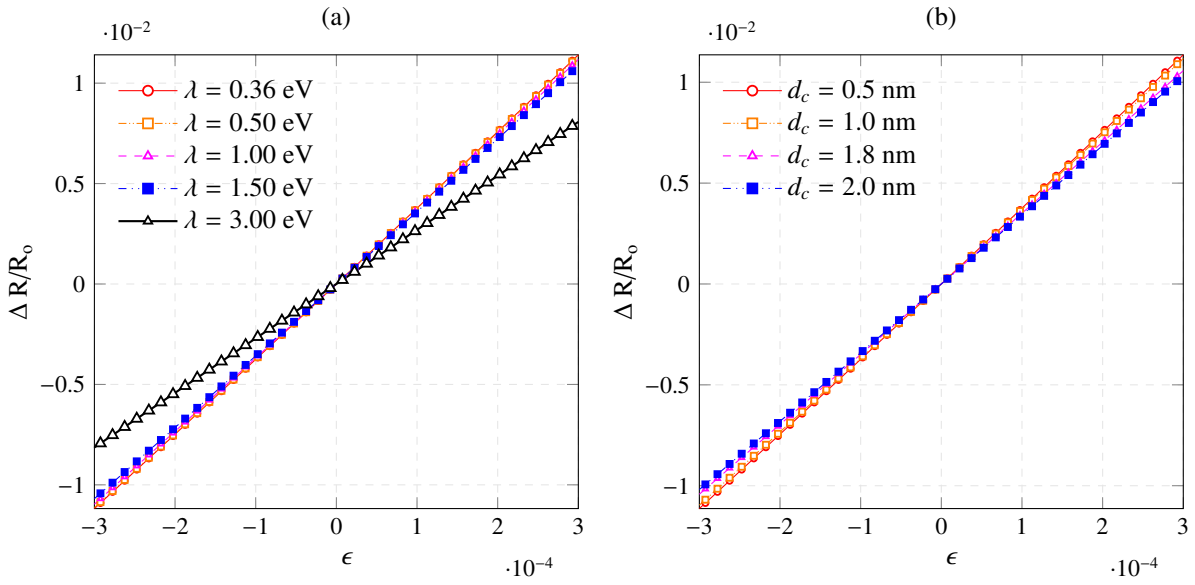

Figure 18: Strain-induced relative resistance change $\Delta R/R_o$ of MWCNT reinforced cement paste for different heights of the potential barrier λ (a), and different critical separation distances (b) (PA, f=0.695%, ν=0.2, L = 1 μm, D=10 nm, σ_c = 10^4 S/m, C_1=8.9045, C_2=0.0243).

Finally, Figs. 19(a) and 19(b) show the relative resistance change for different values of MWCNT conductivity and two filler concentrations, f = 0.69% and f = 2%, respectively. It can be extracted from these figures that more conductive fillers lead to higher strain sensitivities. Another noticeable aspect is that the nonlinearities, related to the coupled effect of the volume expansion and variation of the percolation threshold, gain importance for concentrations close to the unloaded percolation threshold. On the contrary, the strain-sensing curves exhibit more linear behaviors for concentrations far from this critical concentration. In other words, when the filler concentration is near the percolation threshold, the number of formed conductive paths is still limited so that the breakage or formation of conductive networks has a large impact on the overall conductivity. However, when there exist many conductive paths, the variation of the number of paths does not lead to substantial differences and the composite is thus less piezoresistive. From a mathematical point of view, the strain-induced variations of the effective volume fraction f^* and of the percolation threshold f_c result in a variation of the fraction of percolated CNTs ξ defined in Eq. (12). Hence, the appearance of a nonlinear response for concentrations close to the percolation threshold is justified by the percolation theory. When percolation begins, i.e. for small values of ξ, the conductivity of CNT reinforced nanocomposites experiences a sharp increase. Once a sufficient number of conductive paths has been formed, the effective conductivity stabilizes. In this first region is where the strain-induced changes lead to the largest impacts and the most nonlinear effects.

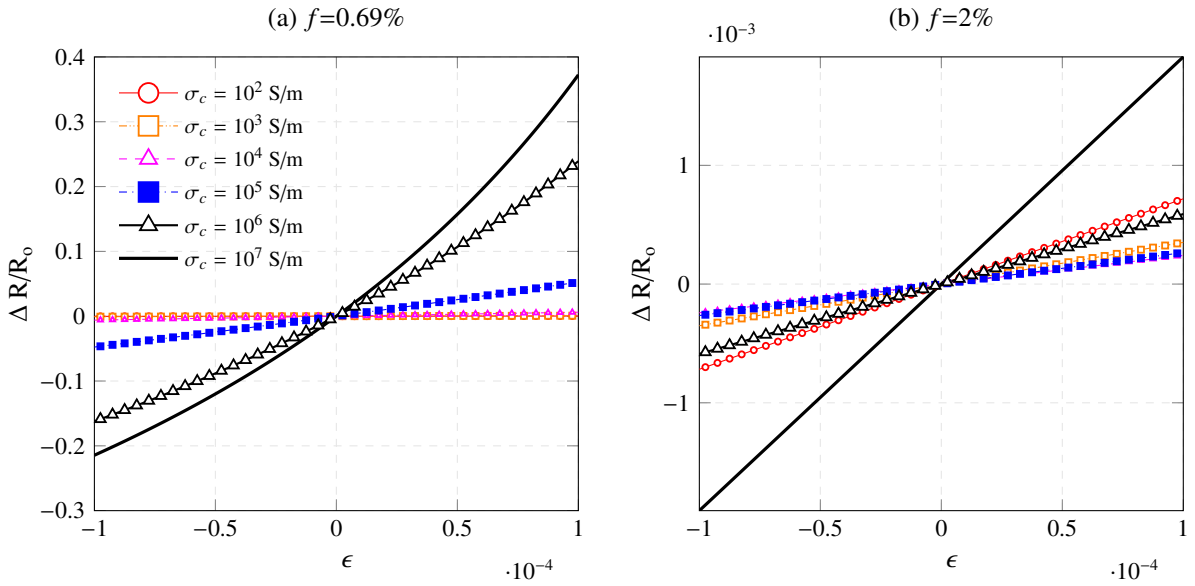

Figure 19: Strain-induced relative resistance change $\Delta R/R_o$ of MWCNT reinforced cement paste for different filler conductivities σ_c and volume fraction f = 0.69% (a), and f = 2% (b) (PA, ν=0.2, L = 1 μm, D=10 nm, λ=0.36 eV, d_c=0.5 nm, C_1=8.9045, C_2=0.0243).

4.2.2. Effects of MWCNTs waviness

In this section, the effect of MWCNTs waviness on the piezoresistive properties of the composites is investigated. Five wavy geometries, corresponding to helical angles of 90, 80, 70, 60 and 50°, have been considered. Figs. 20(a) and 20(b) show the relative resistance variation for filler concentrations of 1 and 2%, respectively. The main effect of non-straightness of the fibers is an increase of the percolation threshold as a result of the reduction of the length from the wavy to the equivalent straight fiber. As a result, wavy geometries lead to effective volume fractions closer to the percolation threshold and therefore higher values of sensitivity. However, if the geometry is too curved it may result in an effective volume fraction under the percolation threshold and, thus, the strain-sensitivity can get substantially reduced. This is the case of θ = 50° in Fig. 20(a).

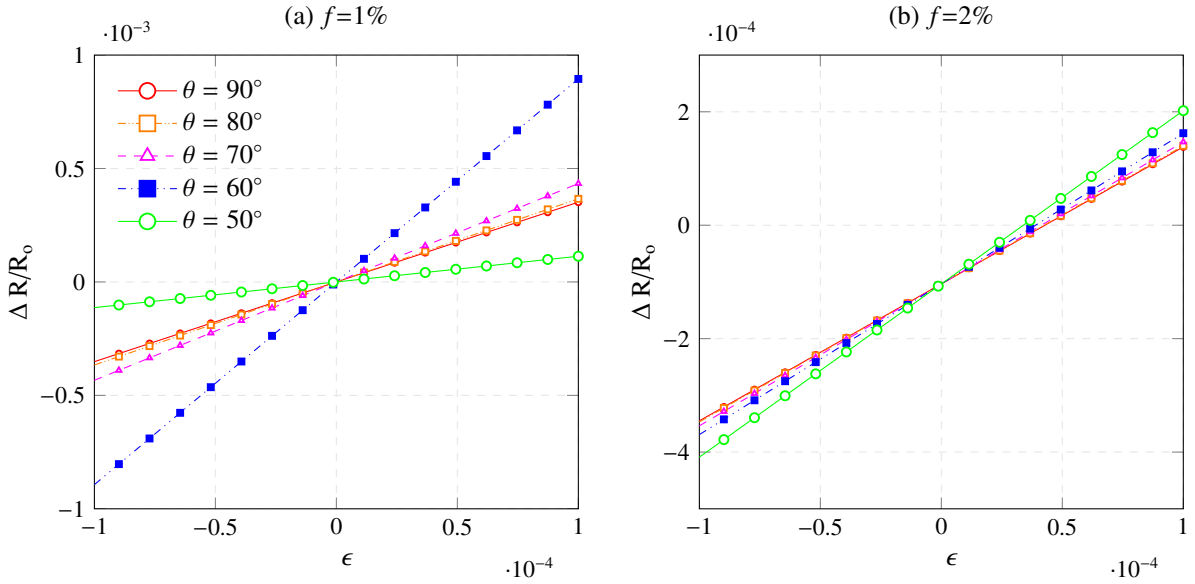

Figure 20: Strain-induced relative resistance change $\Delta R/R_o$ of MWCNT reinforced cement paste for different helical angles θ and volume fraction f = 1% (a), and f = 2% (b) (PA, ν=0.2, L^{wavy}_{CNT} = 1 μm, D=10 nm, λ=0.36 eV, d_c=0.5 nm, σ_c = 10^4 S/m, C_1=8.9045, C_2=0.0243).

4.2.3. Effects of MWCNTs agglomeration

The effect of MWCNTs agglomeration in spherical bundles ($a_1 = a_2 = a_3$) on the conductivity of cement-based composites has been also analyzed. Figs. 21(a) and 21(b) show the relative resistance change for different agglomeration parameters χ and filler concentrations of $f = 1\%$ and $f = 2\%$, respectively. In these analyses, the volume fraction of MWCNTs within the bundles is kept constant at 90% ($\zeta = 0.9$), whereas the ratio between the volume of the bundles and the total volume of the RVE varies from 10 to 90%. Secondly, in Figs. 21(a) and 21(b) the volume fraction of the bundles is set to 40% and the ratio of MWCNTs concentration within them ranges from 40 to 90%. In Fig. 21(a) it is quite clear that the lesser is the value of χ, i.e. the lesser is the volume of the bundles, the lesser is also the piezoresistivity of the composite. Nevertheless, for volume fractions far away from the percolation threshold, as in Fig. 21(b), this effect is not so clear. Depending on the relative volume fraction of both phases, bundles and surrounding composite, the strain sensitivity may substantially vary.

In Fig. 22(a) it can be seen that the variation from the uniform distribution, $\chi = \zeta$=0.4, to the next degree of agglomeration, ζ=0.6, leads to a higher sensitivity of the composite. However, if this value goes on increasing, such as for ζ=0.8 and ζ=0.9, the effective volume fraction within the bundles moves far away from the percolation threshold and the resulting composite exhibits lesser piezoresistivity. On the contrary, for a global volume fraction far away from the percolation threshold as in Fig. 22(b), the effect of the increment of ζ, i.e. increments of the filler concentration within the bundles, clearly reduces the resulting piezoresistivity.

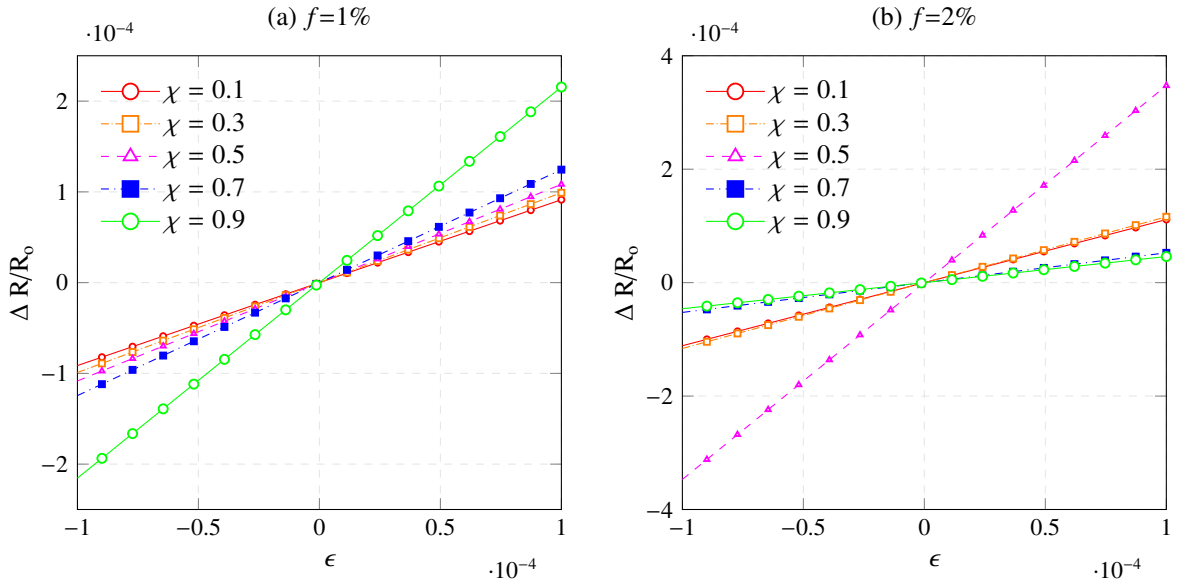

Figure 21: Strain-induced relative resistance change $\Delta R/R_o$ of MWCNT reinforced cement paste for different agglomeration parameters χ and volume fraction $f = 1\%$ (a), and $f = 2\%$ (b) (PA, ζ=0.9, ν=0.2, $L = 1$ μm, D=10 nm, λ=0.36 eV, d_c=0.5 nm, $\sigma_c = 10^5$ S/m, C_1=8.9045, C_2=0.0243).

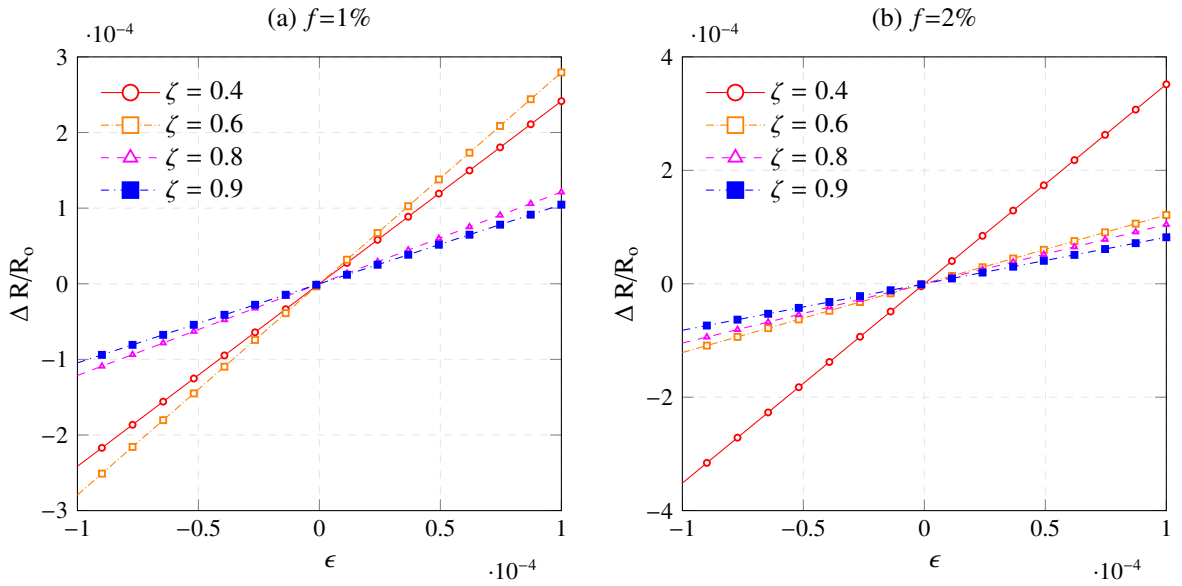

Figure 22: Strain-induced relative resistance change $\Delta R/R_o$ of MWCNT reinforced cement paste for different agglomeration parameters ζ and volume fraction f = 1% (a), and f = 2% (b) (PA, χ=0.4, ν=0.2, L = 1 μm, D=10 nm, λ=0.36 eV, d_c=0.5 nm, σ_c = 10^5 S/m, C_1=8.9045, C_2=0.0243).

4.2.4. Characterization of the gauge factor

As mentioned above, the correlation between measured resistance and strain can be modeled, as a first approximation, by means of the same formula used for conventional strain gauges (Eq. 38). However, because of the peculiar electromechanical behavior of MWCNT reinforced composites, the gauge factor λ is rate dependent and also varies with ϵ, resulting in a nonlinear relationship of strain-to-signal. As it was already shown in Fig. 19, as well as it has been evidenced in some other previously published experimental and theoretical works [97], the strain-sensing curves can be approximately modeled with a first linear range followed by a nonlinear one. Although there are a few works dealing with the definition of the nonlinear part, such as the work of Park et al. [97] who defined it by an exponential-type function, the linear part is of high interest in the realm of SHM as the accuracy of the measurements is higher within this range. In this work, a linear regression based on a least squares estimator is adjusted in the strain range leading to a coefficient of determination of 0.99, as schematically represented in Fig. 23(a). Hence, two different gauge factors, λ^- and λ^+, can be extracted from the slope of both linear fittings for compressive and tensile strains, respectively, as follows:

$$\frac{\Delta R}{R_o} = \lambda^- \epsilon, \quad \epsilon < 0 \tag{39a}$$

$$\frac{\Delta R}{R_o} = \lambda^+ \epsilon, \quad \epsilon > 0 \tag{39b}$$

On this basis, the variation of the gauge factor with the filler concentration can be obtained as shown in Fig. 23(b). It should be noted that the gauge factor is slightly higher in the case of tensile stresses. In this case, the percolation threshold increases with increasing inter-particle distance and with volume expansion. However, in the case of compressive strains, the percolation threshold also increases whilst the rest of the parameters decrease (see Fig. 17). Moreover, according to results of Fig. 14, a maximum value of the gauge factor is observed around the percolation threshold. Figs. 24(a) and 24(b) depict the gauge factor of MWCNT reinforced cement paste with different filler concentrations under compressive and tensile strains, respectively. As expected from Fig. 19 more conductive fillers lead to higher gauge factor values. It is also noticeable that for higher filler conductivities the peaks are sharper, whilst lower filler conductivities lead to smoother curves.

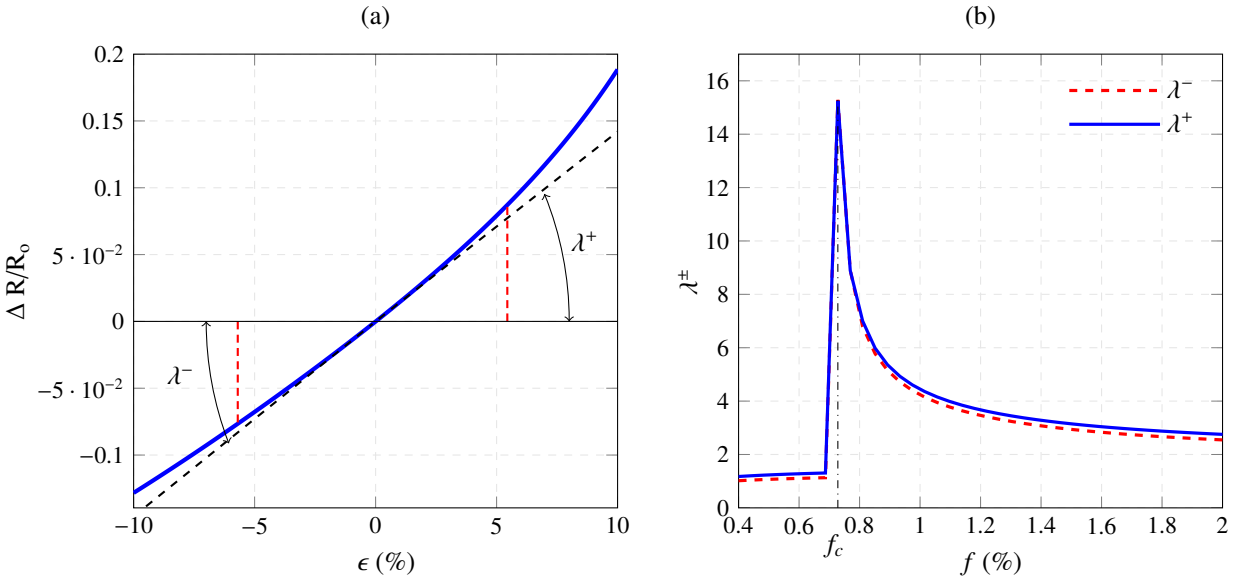

Figure 23: Characterization of the gauge factor and the linear strain gauge range (a), and strain gauge of MWCNT reinforced cement paste versus filler concentration f under compressive λ^- and tensile λ^+ strains (b) (ν=0.2, L = 1 μm, D=10 nm, λ=0.36 eV, d_c=0.56 nm, σ_c = 10^5 S/m, C_1=8.9045, C_2=0.0243).

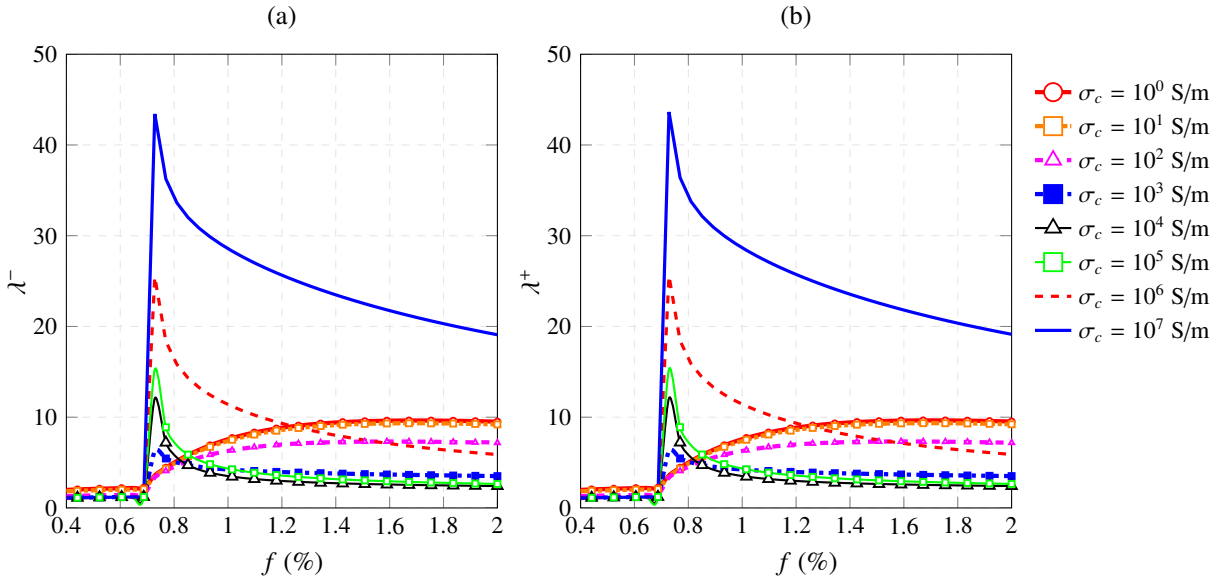

Figure 24: Strain gauge of MWCNT reinforced cement paste versus filler concentration f under compressive λ^- (a) and tensile λ^+ strains (b), for different filler conductivities σ_c (ν=0.2, L = 1 μm, D=10 nm, λ=0.36 eV, d_c=0.56 nm, σ_c = 10^5 S/m, C_1=8.9045, C_2=0.0243).

4.3. Experimental validation

On the basis of the previous analyses, the proposed micromechanics approach has been compared to the experimental results obtained for different cement-based composites. Fig. 25 shows some examples of time histories of applied strain and corresponding electrical resistance obtained in the experiments. In particular, the figures show the response of paste, mortar and concrete specimens containing a filler concentration of 1.5, 1 and 1% with respect to cement weight, respectively. Hence, according to Eq. (38), the values of the gauge factor obtained from the strain sensing tests are compared to the values obtained by the proposed approach in Fig. 26. The CNT electrical conductivity has been set between 10^1 and 10^4 S/m. The SEM inspections in the analyzed specimens showed good dispersions of the nanoinclusions in the cementitious matrices. This fact has been verified numerically with the use of limited values for the agglomeration parameters with good results of both overall effective conductivity and strain-sensing curves. The values of the agglomeration parameters, waviness, geometric properties of the

fillers, as well as the variation parameters C_1 and C_2 have been adjusted to fit the experimental data. It is observed that the analytical prediction agrees well with the experimental results and the tendency of the gauge factor λ^- is well captured by the current model. The experimental data also show the existence of an optimal content of nanotubes around 0.75-1% mass content with respect to the mass of cement. This behavior is reproduced by the current approach, as shown above in Fig. 14, with the optimal content of nanotubes at the percolation threshold.

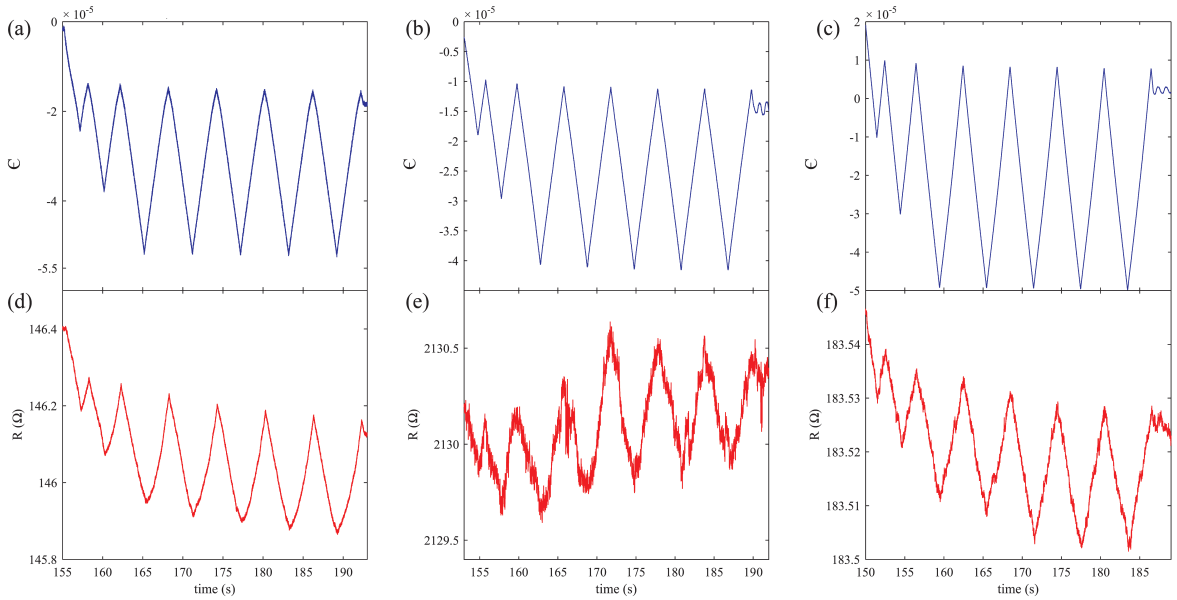

Figure 25: Time histories of applied compression strain and corresponding electrical resistance outputted by (a) paste, (b) mortar and (c) cement specimens with filler concentrations of 1.5, 1 and 1% with respect to cement weight, respectively.

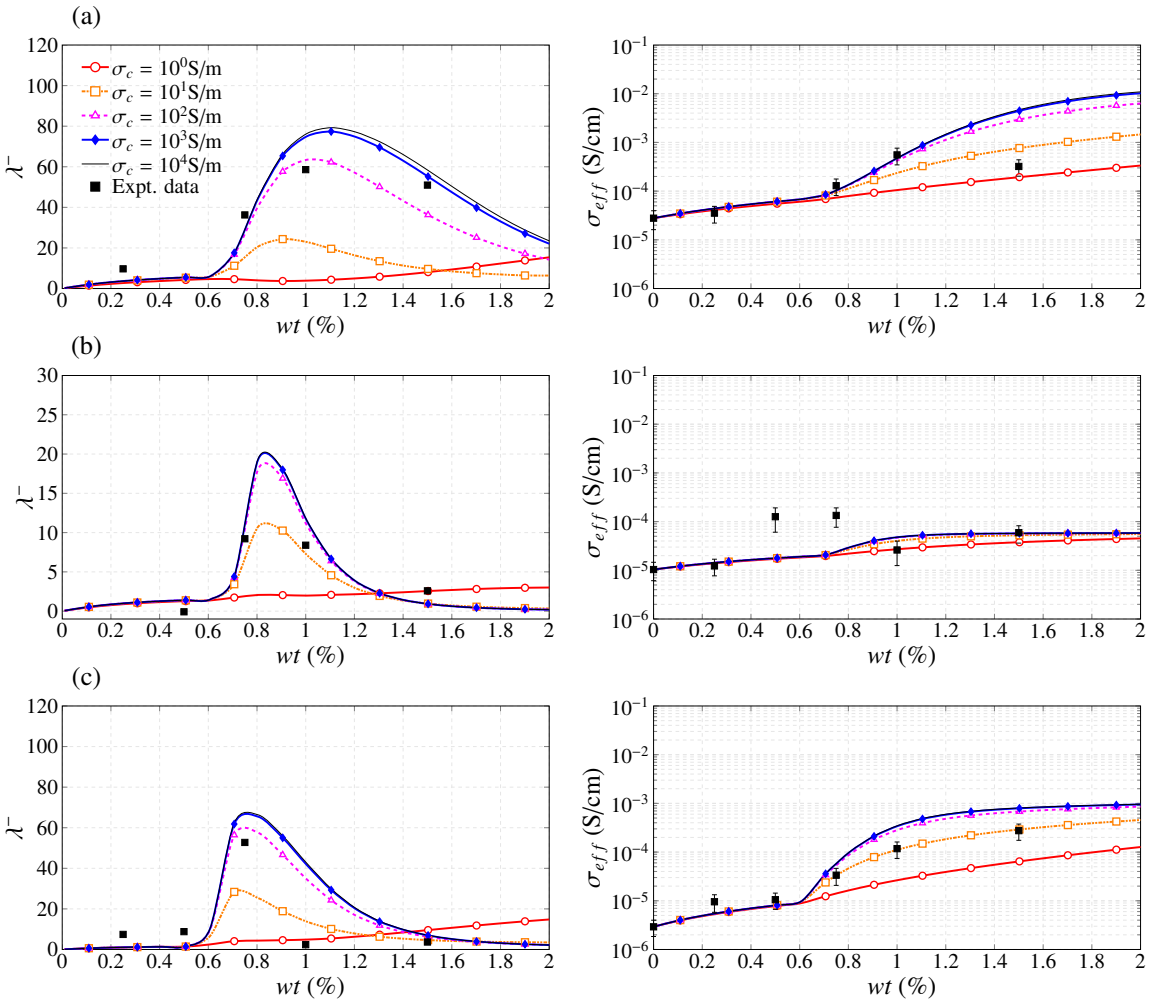

Figure 26: Comparison of the theoretical predictions and the experimental electrical compression gauge factors λ^- for cement-based sensors. ((a) PA, L = 0.25 μm, D=10 nm, λ=0.56 eV, d_c=1.8 nm, χ=0.90, ζ=0.90, θ=35°, C_1=6.8, C_2=1.7; (b) MO, L = 0.25 μm, D=10 nm, λ=0.56 eV, d_c=1.8 nm, χ=0.68, ζ=0.90, θ=40°, C_1=5.2, C_2=1.5; (c) CO, L = 0.25 μm, D=10 nm, λ=0.56 eV, d_c=1.8 nm, χ=0.90, ζ=0.90, θ=69°, C_1=5.0, C_2=1.5)

Fig. 27 shows the comparison in the $R-\epsilon$ plane for three samples of cement paste, mortar and concrete with filler concentrations of 1, 0.75 and 0.75% with respect to the mass of cement, respectively. The material properties have been taken from Fig. 26. In order to compare the effective conductivity of the composites from Eq. (13) in the direction of application of the external strain, σ^{22}_{eff}, with the electrical resistance, R, measured in the specimens through a high precision LCR meter, the following relation was applied:

$$\sigma^{22}_{eff} = \frac{d}{AR} \tag{40}$$

being A the specimen's cross-section and d the electrode's distance with values of 51 × 51 mm^2 and 10 mm, respectively (see Fig. 10). It is noted in this figure that the presented approach can simulate fairly well the linear part of the strain-sensing curves for the three different matrices. According to the results of Fig. 26, a filler conductivity around 10^2 S/m leads to very proximate values of the gauge factor. However, for the considered range of small deformations, the appearance of stronger contributions of non-linearities, associated with the variation of the percolation threshold, were not captured by the proposed method. This is the case of cement-paste and concrete specimens, where only the linear behavior was captured by the proposed approach. In the case of mortar specimens, the strain-sensing curve is prominently linear and the theoretical approach provides very proximate values.

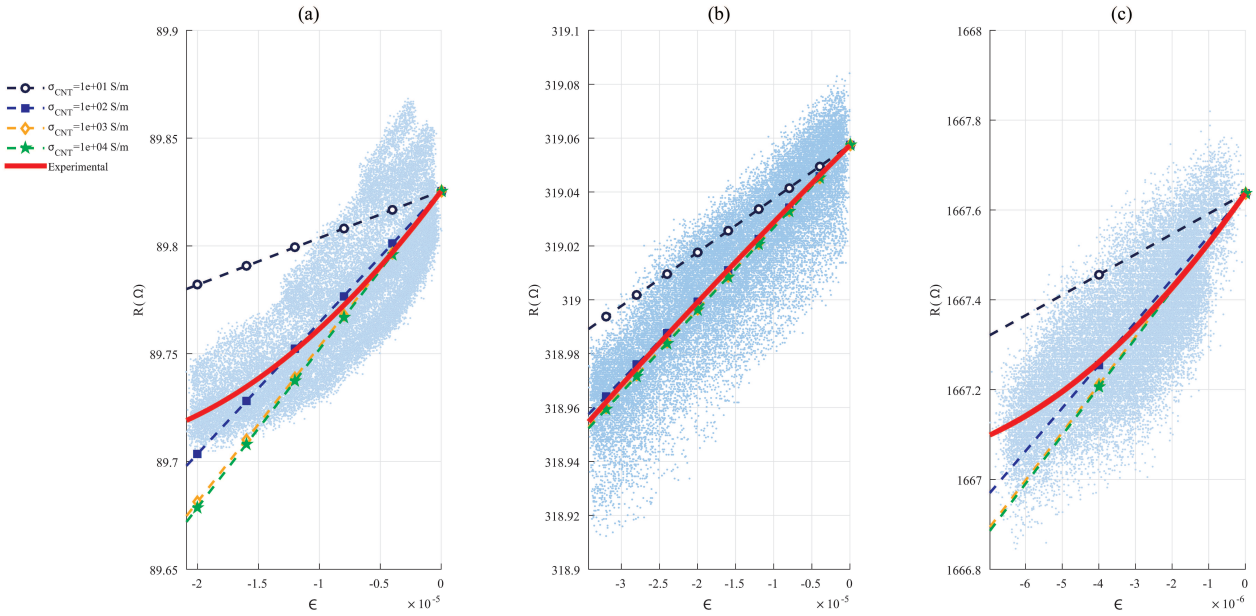

Figure 27: Comparison of the theoretical predictions and the experimental electrical resistance versus applied strain for (a) paste, (b) mortar and (c) cement specimens with filler concentrations of 1, 0.75 and 0.75% with respect to cement weight, respectively.

5. Conclusions

This paper has presented a micromechanics model to predict the piezoresistive properties of CNT cement-based nanocomposites with the consideration of waviness and non-uniform spatial distributions of nanoinclusions. The two mechanisms that contribute to the conductivity of CNT composites, namely electron hopping and conductive networks, have been contemplated in the mixed micromechanics framework. The origin of the piezoresistive response of these composites has been attributed to strain-induced changes in the volume fraction, changes in the conductive networks due to the filler reorientation and, therefore, the percolation threshold, and, finally, changes in the tunneling resistance through variation of the inter-particle distance and the height of the potential barrier. The Komoro and Makishima's stochastic method has been implemented in order to evaluate the variation of the percolation threshold following an applied strain through the resulting strain-induced orientation distribution function (ODF). Moreover, a helical waviness model and a two-parameter agglomeration approach have been proposed.

In order to count on an experimental basis to use as benchmark to validate the analytical model, several nanocomposite cement-based specimens have been manufactured and tested. In particular, specimens of cement pastes, mortars and concretes with different concentrations of MWCNTs have been prepared. The quality of the dispersion has been evaluated using scanning electron microscopy.

Detailed parametric analyses have been carried out in order to illustrate the influence of the properties of the constituents, waviness and agglomeration. In order to highlight the importance of the tunneling effect in the piezoresistivity of MWCNT cement-based composites, the influence of the variation of the height of the tunneling potential barrier and the inter-particle distance have been analyzed. Furthermore, the effects of non-uniform spatial distributions of MWCNTs have been evaluated through the proposed two-parameters agglomeration model. Finally, the accuracy of the proposed approach has been demonstrated by comparison with the experimental data from the tested specimens.

The main contributions of this paper are summarized below.

- The strain-sensing capability of MWCNT cement-based composites critically depends on the MWCNT content. Both experiments and theoretical modeling confirm that the largest gauge factors are achieved at the percolation threshold.
- The nonlinear relationship between ohmic resistance and externally applied strains is related to the variation of the percolation threshold. Specimens with filler contents close to the percolation threshold exhibit higher levels of nonlinearity, whilst specimens having concentrations far from this critical value tend to exhibit a more linear behavior.
- More conductive fillers lead to higher strain-gauges. In addition, the importance of the non-linear behavior increases with increasing fillers conductivity.

- The comparison of the analytical predictions against experimental data demonstrates that the presented mixed micromechanics model can predict fairly well the gauge factor of MWCNT cement-based composites. Furthermore, the incorporation of waviness and agglomeration enhanced the analytical results.
- The results also showed that the presented approach can model the linear range of piezoresistivity, useful for the development of monitoring applications of CNT cement-based nanocomposites in the realm of SHM. Moreover, the proposed approach also proved capable to model the non-linear response associated with the variation of the percolation threshold, similar to experimental evidence. However, some discrepancies have been found in some specimens with filler contents close to the percolation threshold. These differences are hypothesized to be due to the consideration of uniform average distance among nanotubes. However, this approach offers a suitable framework in which incorporate more complex distributions in further research.

The presented micromechanics model is envisaged to provide a useful tool for the understanding of the physical mechanisms that govern the piezoresistive behavior of MWCNT cement-based composites. Furthermore, this analytical approach generates quantitative predictions, valuable for the design of these composites with a reduced computational cost. Finally, this model gives an analytical framework suitable for the incorporation of uncertainties of the constituents properties, waviness and agglomeration, interesting for future research on stochastic design of MWCNT cement-based composites. In order to develop a fully independent designing tool, further research must be pursued on the determination of the initial inter-particle distance and the height of the potential barrier, as well as the strain-induced variation parameters, namely C_1 and C_2. Furthermore, the presented two-parameters agglomeration model is suitable to be extended in the realm of multi-inclusion models. Hence, statistical distributions can be used in order to evaluate the piezoresistive behavior of more realistic non-uniform distributions of nanotubes.

Acknowledgement

This work was partially financed by the Ministerio de Economía y Competitividad of Spain under the project DPI2014-53947-R. E. G-M was also supported by a FPU contract-fellowship from the Spanish Ministry of Education Ref: FPU13/04892. The support of the Italian Ministry of Education, University and Research (MIUR) through the funded Project of Relevant National Interest "SMART-BRICK: Novel strain-sensing nano-composite clay brick enabling self-monitoring masonry structures" is also gratefully acknowledged.

References

[1] J. M. Brownjohn, Structural health monitoring of civil infrastructure, Philosophical Transactions of the Royal Society of London A: Mathematical, Physical and Engineering Sciences 365 (2007) 589–622.

[2] B. Culshaw, Structural health monitoring of civil engineering structures, Progress in Structural Engineering and Materials 1 (1998) 308–315.

[3] B. Han, X. Yu, E. Kwon, A self-sensing carbon nanotube/cement composite for traffic monitoring, Nanotechnology 20 (2009) 445501.

[4] F. Ubertini, A. L. Materazzi, A. D'Alessandro, S. Laflamme, Natural frequencies identification of a reinforced concrete beam using carbon nanotube cement-based sensors, Engineering Structures 60 (2014) 265–275.

[5] A. D. B. Ferreira, P. R. Nóvoa, A. T. Marques, Multifunctional material systems: A state-of-the-art review, Composite Structures (2016).

[6] O. Galao, F. Baeza, E. Zornoza, P. Garcés, Strain and damage sensing properties on multifunctional cement composites with CNF admixture, Cement and concrete composites 46 (2014) 90–98.

[7] S. Laflamme, F. Ubertini, H. Saleem, A. D'Alessandro, A. Downey, H. Ceylan, A. L. Materazzi, Dynamic characterization of a soft elastomeric capacitor for structural health monitoring, Journal of Structural Engineering 141 (2014) 04014186.

[8] F. Ubertini, S. Laflamme, A. D'Alessandro, Smart cement paste with carbon nanotubes, Innovative Developments of Advanced Multifunctional Nanocomposites in Civil and Structural Engineering (2016) 97–120.

[9] H. Li, H. Xiao, J. Ou, A study on mechanical and pressure-sensitive properties of cement mortar with nanophase materials, Cement and Concrete research 34 (2004) 435–438.

[10] B. Han, Y. Wang, S. Dong, L. Zhang, S. Ding, X. Yu, J. Ou, Smart concretes and structures: A review, Journal of intelligent material systems and structures 26 (2015) 1303–1345.

[11] T. Hou, J. Lynch, Conductivity-based strain monitoring and damage characterization of fiber reinforced cementitious structural components, in: Proc. SPIE, volume 5765, pp. 419–429.

[12] S. P. Shah, M. Konsta-Gdoutos, Z. Metaxa, P. Mondal, Nanoscale modification of cementitious materials, in: Nanotechnology in Construction 3, Springer, 2009, pp. 125–130.

[13] B. Han, X. Guan, J. Ou, Electrode design, measuring method and data acquisition system of carbon fiber cement paste piezoresistive sensors, Sensors and Actuators A: Physical 135 (2007) 360–369.

[14] B. Han, X. Yu, J. Ou, Multifunctional and smart carbon nanotube reinforced cement-based materials, in: Nanotechnology in civil infrastructure, Springer, 2011, pp. 1–47.

[15] B. Han, S. Ding, X. Yu, Intrinsic self-sensing concrete and structures: A review, Measurement 59 (2015) 110–128.

[16] E. García-Macías, R. Castro-Triguero, E. I. S. Flores, M. I. Friswell, R. Gallego, Static and free vibration analysis of functionally graded carbon nanotube reinforced skew plates, Composite Structures (2016).

[17] D. Ürk, E. Demir, O. Bulut, D. Çakıroğlu, F. Ç. Cebeci, M. L. Öveçoğlu, H. Cebeci, Understanding the polymer type and CNT orientation effect on the dynamic mechanical properties of high volume fraction CNT polymer nanocomposites, Composite Structures 155 (2016) 255–262.

[18] D. Savvas, G. Stefanou, V. Papadopoulos, M. Papadrakakis, Effect of waviness and orientation of carbon nanotubes on random apparent material properties and RVE size of CNT reinforced composites, Composite Structures (2016).

[19] T. Üstün, V. Eskizeybek, A. Avci, Enhanced fatigue performances of hybrid nanoreinforced filament wound carbon/epoxy composite pipes, Composite Structures 150 (2016) 124–131.

[20] L. Zhang, K. Liew, J. Reddy, Postbuckling analysis of bi-axially compressed laminated nanocomposite plates using the first-order shear deformation theory, Composite Structures 152 (2016) 418–431.

[21] B. Chen, K. Wu, W. Yao, Conductivity of carbon fiber reinforced cement-based composites, Cement and Concrete Composites 26 (2004) 291–297.

[22] M. Chiarello, R. Zinno, Electrical conductivity of self-monitoring CFRC, Cement and Concrete Composites 27 (2005) 463–469.

[23] S. Wen, D. Chung, Double percolation in the electrical conduction in carbon fiber reinforced cement-based materials, Carbon 45 (2007) 263–267.

[24] S. Wen, D. Chung, Carbon fiber-reinforced cement as a thermistor, Cement and Concrete Research 29 (1999) 961–965.

[25] H. Li, H. Xiao, J. Ou, Effect of compressive strain on electrical resistivity of carbon black-filled cement-based composites, Cement and Concrete Composites 28 (2006) 824–828.

[26] L. Chang, K. Friedrich, L. Ye, P. Toro, Evaluation and visualization of the percolating networks in multi-wall carbon nanotube/epoxy composites, Journal of materials science 44 (2009) 4003–4012.

[27] C. Feng, L. Jiang, Investigation of uniaxial stretching effects on the electrical conductivity of CNT-polymer nanocomposites, Journal of Physics D: Applied Physics 47 (2014) 405103.

[28] N. Hu, H. Fukunaga, S. Atobe, Y. Liu, J. Li, Piezoresistive strain sensors made from carbon nanotubes based polymer nanocomposites, Sensors 11 (2011) 10691–10723.

[29] G. T. Pham, Y. Park, Z. Liang, C. Zhang, B. Wang, Processing and modeling of conductive thermoplastic/carbon nanotube films for strain sensing, Composites Part B: Engineering 39 (2008) 209–216.

[30] S. Gong, Z. H. Zhu, On the mechanism of piezoresistivity of carbon nanotube polymer composites, Polymer 55 (2014) 4136–4149.

[31] Q. Cheng, J. Bao, J. Park, Z. Liang, C. Zhang, B. Wang, High mechanical performance composite conductor: multi-walled carbon nanotube sheet/bismaleimide nanocomposites, Advanced Functional Materials 19 (2009) 3219.

[32] X. Wang, P. D. Bradford, W. Liu, H. Zhao, Y. Inoue, J. Maria, Q. Li, F. Yuan, Y. Zhu, Mechanical and electrical property improvement in CNT/nylon composites through drawing and stretching, Composites Science and Technology 71 (2011) 1677–1683.

[33] A. Ameli, P. Jung, C. Park, Electrical properties and electromagnetic interference shielding effectiveness of polypropylene/carbon fiber composite foams, Carbon 60 (2013) 379–391.

[34] C. Lin, H. Wang, W. Yang, Variable percolation threshold of composites with fiber fillers under compression, Journal of Applied Physics 108 (2010) 013509.

[35] F. Grillard, C. Jaillet, C. Zakri, P. Miaudet, A. Derré, A. Korzhenko, P. Gaillard, P. Poulin, Conductivity and percolation of nanotube based polymer composites in extensional deformations, Polymer 53 (2012) 183–187.

[36] X. Zeng, X. Xu, P. M. Shenai, E. Kovalev, C. Baudot, N. Mathews, Y. Zhao, Characteristics of the electrical percolation in carbon nanotubes/polymer nanocomposites, The Journal of Physical Chemistry C 115 (2011) 21685–21690.

[37] B. Zhang, Z. Zhou, K. Zhang, G. Yan, Z. Xu, Sensitive skin and the relative sensing system for real-time surface monitoring of crack in civil infrastructure, Journal of intelligent material systems and structures 17 (2006) 907–917.

[38] K. Loh, T. Hou, J. Lynch, N. Kotov, Nanotube-based sensing skins for crack detection and impact monitoring of structures, in: Proceedings of the 6th International Workshop on Structural Health Monitoring, Stanford, CA, USA.

[39] N. Hu, Y. Karube, M. Arai, T. Watanabe, C. Yan, Y. Li, Y. Liu, H. Fukunaga, Investigation on sensitivity of a polymer/carbon nanotube composite strain sensor, Carbon 48 (2010) 680–687.

[40] R. Howser, H. Dhonde, Y. Mo, Self-sensing of carbon nanofiber concrete columns subjected to reversed cyclic loading, Smart materials and structures (2011).

[41] M. S. Konsta-Gdoutos, C. A. Aza, Self sensing carbon nanotube (CNT) and nanofiber (CNF) cementitious composites for real time damage assessment in smart structures, Cement and Concrete Composites 53 (2014) 162–169.

[42] F. Ubertini, S. Laflamme, H. Ceylan, A. L. Materazzi, G. Cerni, H. Saleem, A. D'Alessandro, A. Corradini, Novel nanocomposite technologies for dynamic monitoring of structures: a comparison between cement-based embeddable and soft elastomeric surface sensors, Smart Materials and Structures 23 (2014) 045023.

[43] A. D'Alessandro, M. Rallini, F. Ubertini, A. L. Materazzi, J. M. Kenny, Investigations on scalable fabrication procedures for self-sensing carbon nanotube cement-matrix composites for SHM applications, Cement and Concrete Composites 65 (2016) 200–213.

[44] B. Han, B. Han, J. Ou, Experimental study on use of nickel powder-filled portland cement-based composite for fabrication of piezoresistive sensors with high sensitivity, Sensors and Actuators A: Physical 149 (2009) 51–55.

[45] A. D'Alessandro, F. Ubertini, A. L. Materazzi, S. Laflamme, M. Porfiri, Electromechanical modelling of a new class of nanocomposite cement-based sensors for structural health monitoring, Structural Health Monitoring (2014) 1475921714560071.

[46] B. Han, K. Zhang, X. Yu, E. Kwon, J. Ou, Electrical characteristics and pressure-sensitive response measurements of carboxyl MWNT/cement composites, Cement and Concrete Composites 34 (2012) 794–800.

[47] F. Deng, Q. Zheng, An analytical model of effective electrical conductivity of carbon nanotube composites, Applied Physics Letters 92 (2008) 071902.

[48] T. Takeda, Y. Shindo, Y. Kuronuma, F. Narita, Modeling and characterization of the electrical conductivity of carbon nanotube-based polymer composites, Polymer 52 (2011) 3852–3856.

[49] G. D. Seidel, D. C. Lagoudas, A micromechanics model for the electrical conductivity of nanotube-polymer nanocomposites, Journal of Composite Materials 43 (2009) 917–941.

[50] C. Feng, L. Jiang, Micromechanics modeling of the electrical conductivity of carbon nanotube (CNT)–polymer nanocomposites, Composites Part A: Applied Science and Manufacturing 47 (2013) 143–149.

[51] T. Mori, K. Tanaka, Average stress in matrix and average elastic energy of materials with misfitting inclusions, Acta metallurgica 21 (1973) 571–574.

[52] H. Hatta, M. Taya, Effective thermal conductivity of a misoriented short fiber composite, Journal of Applied Physics 58 (1985) 2478–2486.

[53] T. Theodosiou, D. Saravanos, Numerical investigation of mechanisms affecting the piezoresistive properties of CNT-doped polymers using multi-scale models, Composites Science and Technology 70 (2010) 1312–1320.

[54] T. Yasuoka, Y. Shimamura, A. Todoroki, Electrical resistance change under strain of CNF/flexible-epoxy composite, Advanced Composite Materials 19 (2010) 123–138.

[55] L. Y. Alamusi, N. Hu, Numerical simulations on piezoresistivity of CNT/polymer based nanocomposites, Computers Materials & Continua 20 (2010) 101–117.

[56] N. Hu, Y. Karube, C. Yan, Z. Masuda, H. Fukunaga, Tunneling effect in a polymer/carbon nanotube nanocomposite strain sensor, Acta Materialia 56 (2008) 2929–2936.

[57] J. G. Simmons, Electric tunnel effect between dissimilar electrodes separated by a thin insulating film, Journal of applied physics 34 (1963) 2581–2590.

[58] M. Taya, W. Kim, K. Ono, Piezoresistivity of a short fiber/elastomer matrix composite, Mechanics of materials 28 (1998) 53–59.

[59] T. Tallman, K. Wang, An arbitrary strains carbon nanotube composite piezoresistivity model for finite element integration, Applied Physics Letters 102 (2013) 011909.

[60] A. Celzard, E. McRae, C. Deleuze, M. Dufort, G. Furdin, J. Marêché, Critical concentration in percolating systems containing a high-aspect-ratio filler, Physical Review B 53 (1996) 6209.

[61] C. Feng, L. Jiang, Micromechanics modeling of bi-axial stretching effects on the electrical conductivity of CNT-polymer composites, International Journal of Applied Mechanics 7 (2015) 1550005.

[62] M. S. Shaffer, A. H. Windle, Fabrication and characterization of carbon nanotube/poly (vinyl alcohol) composites, Advanced materials 11 (1999) 937–941.

[63] B. Vigolo, A. Penicaud, C. Coulon, C. Sauder, R. Pailler, C. Journet, P. Bernier, P. Poulin, Macroscopic fibers and ribbons of oriented carbon nanotubes, Science 290 (2000) 1331–1334.

[64] R. H. Poelma, X. Fan, Z. Hu, G. Van Tendeloo, H. W. van Zeijl, G. Q. Zhang, Effects of nanostructure and coating on the mechanics of carbon nanotube arrays, Advanced Functional Materials 26 (2016) 1233–1242.

[65] Y. Yi, L. Berhan, A. Sastry, Statistical geometry of random fibrous networks, revisited: waviness, dimensionality, and percolation, Journal of applied physics 96 (2004) 1318–1327.

[66] L. Berhan, A. Sastry, Modeling percolation in high-aspect-ratio fiber systems. ii. the effect of waviness on the percolation onset, Physical Review E 75 (2007) 041121.

[67] F. Fisher, R. Bradshaw, L. Brinson, Fiber waviness in nanotube-reinforced polymer composites: Modulus predictions using effective nanotube properties, Composites Science and Technology 63 (2003) 1689–1703.

[68] A. Allaoui, S. Bai, H. Cheng, J. Bai, Mechanical and electrical properties of a MWNT/epoxy composite, Composites Science and Technology 62 (2002) 1993–1998.

[69] H. Li, H. Xiao, J. Yuan, J. Ou, Microstructure of cement mortar with nano-particles, Composites Part B: Engineering 35 (2004) 185–189.

[70] J. M. Wernik, S. A. Meguid, Recent developments in multifunctional nanocomposites using carbon nanotubes, Applied Mechanics Reviews 63 (2010) 050801.

[71] G. J. Weng, A dynamical theory for the Mori–Tanaka and Ponte Castañeda–Willis estimates, Mechanics of Materials 42 (2010) 886–893.

[72] B. Yang, K. Cho, G. Kim, H. Lee, Effect of CNT agglomeration on the electrical conductivity and percolation threshold of nanocomposites: A micromechanics-based approach, CMES: Computer Modeling in Engineering & Sciences 103 (2014) 343–365.

[73] E. García-Macías, A. D'Alessandro, R. Castro-Triguero, D. Pérez-Mira, F. Ubertini, Micromechanics modeling of the electrical conductivity of carbon nanotube cement-matrix composites, Composites Part B: Engineering 108 (2017) 451–469.

[74] J. D. Eshelby, The determination of the elastic field of an ellipsoidal inclusion, and related problems, Proceedings of the Royal Society of London. Series A. Mathematical and Physical Sciences 241 (1957) 376–396.

[75] J. Eshelby, The elastic field outside an ellipsoidal inclusion, Proceedings of the Royal Society of London. Series A, Mathematical and Physical Sciences (1959) 561–569.

[76] G. M. Odegard, T. S. Gates, Constitutive modeling of nanotube/polymer composites with various nanotube orientations (2002).

[77] M. Taya, Electronic composites: modeling, characterization, processing, and MEMS applications, Cambridge University Press, 2005.

[78] S. Wen, D. Chung, Effect of carbon fiber grade on the electrical behavior of carbon fiber reinforced cement, Carbon 39 (2001) 369–373.

[79] A. Allaoui, S. V. Hoa, M. D. Pugh, The electronic transport properties and microstructure of carbon nanofiber/epoxy composites, Composites Science and Technology 68 (2008) 410–416.

[80] J. G. Simmons, Generalized formula for the electric tunnel effect between similar electrodes separated by a thin insulating film, Journal of Applied Physics 34 (1963) 1793–1803.

[81] K. Yan, Q. Xue, Q. Zheng, L. Hao, The interface effect of the effective electrical conductivity of carbon nanotube composites, Nanotechnology 18 (2007) 255705.

[82] C. Feng, Micromechanics Modeling of the Electrical Conductivity of Carbon Nanotude (CNT)-Polymer Nanocomposites, Ph.D. thesis, University of Western Ontario, 2014.

[83] M. Shiraishi, M. Ata, Work function of carbon nanotubes, Carbon 39 (2001) 1913–1917.

[84] D. Shi, X. Feng, Y. Huang, K. Hwang, H. Gao, The effect of nanotube waviness and agglomeration on the elastic property of carbon nanotube-reinforced composites, Journal of Engineering Materials and Technology 126 (2004) 250–257.

[85] T. Komori, K. Makishima, Numbers of fiber-to-fiber contacts in general fiber assemblies, Textile Research Journal 47 (1977) 13–17.

[86] N. Pan, A modified analysis of the microstructural characteristics of general fiber assemblies, Textile Research Journal 63 (1993) 336–345.

[87] W. Shim, Y. Kwon, S. Jeon, W. Yu, Optimally conductive networks in randomly dispersed CNT: graphene hybrids, Scientific reports 5 (2015).

[88] V. Kumar, A. Rawal, Tuning the electrical percolation threshold of polymer nanocomposites with rod-like nanofillers, Polymer 97 (2016) 295–299.

[89] H. Corte, O. Kallmes, Statistical geometry of a fibrous network, in: The Formation and Structure of Paper, 1962, pp. 13–46.

[90] S. Toll, Packing mechanics of fiber reinforcements, Polymer Engineering & Science 38 (1998) 1337–1350.

[91] X. Zheng, M. G. Forest, R. Vaia, M. Arlen, R. Zhou, A strategy for dimensional percolation in sheared nanorod dispersions, Advanced Materials 19 (2007) 4038–4043.

[92] Y. Kuronuma, T. Takeda, Y. Shindo, F. Narita, Z. Wei, Electrical resistance-based strain sensing in carbon nanotube/polymer composites under tension: analytical modeling and experiments, Composites Science and Technology 72 (2012) 1678–1682.

[93] A. Sobha, S. K. Narayanankutty, Improved strain sensing property of functionalised multiwalled carbon nanotube/polyaniline composites in TPU matrix, Sensors and Actuators A: Physical 233 (2015) 98–107.

[94] A. M. Neville, Properties of concrete, 4th edition, 1995.

[95] Y. Liao, X. Wei, Penetration resistance and electrical resistivity of cement paste with superplasticizer, Materials and structures 47 (2014) 563–570.

[96] T. P. McAndrew, P. Laurent, M. Havel, C. Roger, Arkema graphistrength® multi-walled carbon nanotubes, Technical Proceedings of the 2008 NSTI Nanotechnology Conference and Trade Show, NSTI-Nanotech, Nanotechnology 2008 1 (2008) 47–50.

[97] M. Park, H. Kim, J. P. Youngblood, Strain-dependent electrical resistance of multi-walled carbon nanotube/polymer composite films, Nanotechnology 19 (2008) 055705.